

## RESEARCH ARTICLE

# A two-fluid single-column model of turbulent shallow convection. Part II: Single-column model formulation and numerics

John Thurnburn  | Georgios A. Efstathiou  | William A. McIntyre 

Department of Mathematics, College of Engineering, Mathematics and Physical Sciences, University of Exeter, Exeter, UK

**Correspondence**

J. Thurnburn, Department of Mathematics, College of Engineering, Mathematics and Physical Sciences, University of Exeter, Exeter EX4 4QF, UK.  
Email: [j.thurnburn@exeter.ac.uk](mailto:j.thurnburn@exeter.ac.uk)

**Funding information**

Natural Environment Research Council, Grant/Award Numbers: NE/N013123/1, NE/T003863/1; Weather and Climate Science for Service Partnership Southeast Asia, Grant/Award Number: SEA21\_2.10

**Abstract**

The two-fluid single-column model of Thurnburn *et al.* (*Quart. J. R. Meteorol. Soc.*, 2019, 145, 1535–1550) is extended to include moisture and horizontal wind shear. Turbulent kinetic energy is introduced as a prognostic variable, dependence on a diagnosed boundary-layer height is removed, and subfilter fluxes are approximated using a two-fluid version of a Mellor–Yamada scheme. Three mechanisms for entrainment and detrainment processes are introduced, which represent entrainment of unstable air at the surface, forced detrainment of air at the top of the boundary/cloud layers, and turbulent mixing that relaxes the convective fluid to a reference profile. A semi-implicit Eulerian discretization replaces the semi-implicit semi-Lagrangian implementation of Thurnburn *et al.* (*Quart. J. R. Meteorol. Soc.*, 2019, 145, 1535–1550) to improve numerical stability and conservation. The equations for the implicit time step are solved using a quasi-Newton method, which is shown to perform well in numerical tests for conservation and convergence. The two-fluid single-column model presented in this article will be applied to simulations of shallow cumulus convection in Part III.

**KEYWORDS**

conditional filtering, multi-fluid modelling, shallow convection

## 1 | INTRODUCTION

The accurate representation of cumulus convection in atmospheric models at unresolved and marginally resolved scales remains a challenge more than five decades after the first convection schemes were developed. The desire to remove some of the restrictive assumptions on which traditional convection schemes are built motivated

the recent introduction of the multi-fluid approach and the closely related extended eddy-diffusivity mass-flux (EDMF) approach; see Tan *et al.* (2018), Thurnburn and Vallis (2018), Thurnburn *et al.* (2018), Weller and McIntyre (2019), Cohen *et al.* (2020), Lopez-Gomez *et al.* (2020), Weller *et al.* (2020), Shipley *et al.* (2022) for discussion. At the same time, there is growing interest in the atmospheric modelling community in improving both the physical

formulation and the numerical techniques used to couple resolved and unresolved processes in numerical models. The multi-fluid and extended EDMF systems have some distinct properties that have required the development of new understanding and new techniques for their numerical solution; see Thuburn *et al.* (2019), Weller and McIntyre (2019), McIntyre *et al.* (2020), and the discussion herein.

This article is the second in a series of three that documents progress in the development of a two-fluid single-column model (SCM) and its application to simulating shallow cumulus convection. Part I (Thuburn *et al.*, 2022) derived the equations for subfilter-scale turbulent second moments. This article presents the new model formulation, including new prognostic equations, closures, and numerics.

Thuburn *et al.* (2019) presented a two-fluid SCM of the dry, shear-free, convective boundary layer (CBL). They showed that the multi-fluid approach can capture some of the essential physics of a convecting fluid and key features of a CBL, including the counter-gradient potential temperature transport in the upper half of the boundary layer, the location of the mean potential temperature minimum in the middle of the boundary layer, and the occurrence of a boundary-layer-top entrainment flux of order 0.1 times the surface potential temperature flux.

However, they also noted several shortcomings of their particular model formulation and implementation:

- The model does not include moist processes and assumes the horizontal wind components to be zero. Thus, it is applicable only to the dry, shear-free regime.
- Some of the parametrized processes in the model (entrainment and detrainment rates, eddy diffusivity) involve specified coefficient profiles that depend on a diagnosed boundary-layer height  $z_{*}$ . These processes result in extremely sharp features in updraft  $w$  and  $\theta$  at the boundary-layer top. Besides being unrealistic, the sharpness of these features inhibits convergence with increasing resolution. Moreover, this formulation introduces non-local dependencies that are difficult to linearize, impacting convergence of the iterative semi-implicit solver.
- In order to eliminate unknowns as far as possible by hand, various approximations are made in the iterative semi-implicit solver; however, these approximations result in slower than ideal convergence of the solver.
- There are several issues with the use of a semi-Lagrangian advection scheme for transport.
  - Conservation of mass and entropy or  $\theta$  imposes important constraints on the growth of the CBL.

The poor conservation of the semi-Lagrangian transport scheme in the presence of sharp features in the  $\theta$  profile leads to large errors unless a fixer is used.

- Semi-Lagrangian advection schemes are most accurate when the Lagrangian time-scale is long. However, in the CBL, particularly near the surface, the Eulerian time-scale is long but the Lagrangian time-scale is short. The semi-Lagrangian advection scheme poorly captures the balance among several fast processes: diffusion, entrainment, and advection.
- Despite its excellent stability properties when solving the usual compressible Euler equations of fluid dynamics, the semi-implicit semi-Lagrangian discretization is in fact unstable when applied to the two-fluid equations (Appendix A).

This article describes the formulation of a new two-fluid SCM that improves on the model of Thuburn *et al.* (2019) in several ways.

- It includes simple moist processes and predicts horizontal wind components, so is applicable to a wider range of regimes.
- Dependence of parametrized terms on a diagnosed  $z_{*}$  has been almost completely removed. Subfilter-scale fluxes and relabelling terms are formulated in terms of various predicted or diagnosed second moments so that their basis, and their behaviour, is more physically realistic. Non-local dependencies have been minimized, improving solver convergence.
- A new solver has been developed that permits more complete coupling between increment equations, improving solver convergence and model stability.
- A semi-implicit Eulerian numerical method is used. It improves conservation properties, is better able to capture balances among fast processes, and is significantly more stable than the previous semi-implicit semi-Lagrangian scheme (Appendix A).

The governing equations for the two-fluid scheme are presented in Section 2. Thermodynamic equations and assumptions are stated in Section 3, and the parametrizations for entrainment, detrainment, subfilter fluxes, and dissipation are given in Section 4. Finally, the numerical methods used for the two-fluid SCM are presented in Section 5, and numerical experiments for conservation and convergence are conducted in Section 6. Simulation results for shallow convection are presented in a companion paper, Part III McIntyre *et al.* (2022).

TABLE 1 Mathematical notation used in this article

| Symbol                      | Formula           | Description   |
|-----------------------------|-------------------|---|
| $\Phi$                      | $gz$              | Geopotential  |
| $f$                         |                   | Coriolis parameter  |
| $u_g, v_g$                  |                   | Imposed geostrophic wind components   |
| $p$                         |                   | Filter-scale pressure (same in both fluids)   |
| $\sigma_i$                  |                   | Filter-scale volume fraction of fluid $i$   |
| $\rho_i$                    |                   | Filter-scale density of fluid $i$   |
| $m_i$                       | $\sigma_i \rho_i$ |   |
| $\rho$                      | $\sum_i m_i$      | Mean density over all fluids  |
| $\eta_i$                    |                   | Filter-scale entropy of fluid $i$   |
| $q_i$                       |                   | Filter-scale total specific humidity of fluid $i$   |
| $u_i, v_i, w_i$             |                   | Filter-scale velocity components of fluid $i$   |
| $T_i$                       |                   | Filter-scale temperature of fluid $i$   |
| $F_i$                       | $m_i w_i$         | Vertical mass flux in fluid $i$   |
| $F_{SF}^{\psi_i}$           |                   | Subfilter-scale vertical flux of $\psi$ in fluid $i$  |
| $\mathcal{P}_i$             |                   | Vertical drag due to subfilter-scale pressure fluctuations  |
| $\mathcal{M}_{ij}$          |                   | Filter-scale rate per unit volume at which mass is relabelled from type $j$ to type $i$   |
| $\hat{\psi}_{ij}$           |                   | Mean value of any variable $\psi$ in fluid that is relabelled from type $j$ to type $i$   |
| $\mathcal{F}^{\text{PROC}}$ |                   | Tunable parameter that controls the mass relabelling rate for a given process   |
| $b_{\psi,ij}^{\text{PROC}}$ |                   | Tunable parameter that controls $\hat{\psi}_{ij}$ for a given process   |
| $C_i^{\psi\phi}$            |                   | Subfilter-scale (co)variance of $\psi$ and $\phi$ in fluid $i$  |
| $k_i$                       |                   | Subfilter-scale turbulent kinetic energy (TKE) in fluid $i$   |
| $\mathcal{R}_i^{\psi\phi}$  |                   | Net effect of the relabelling terms $\mathcal{M}$ on $C_i^{\psi\phi}$   |
| $R_i^{\psi}$                |                   | Additional effective relabelling effect on any variable $\psi$ associated with vertical subfilter-scale fluxes and vertical variation of $\sigma_i$                                     |
| $R_i^{\psi\phi}$            |                   | Additional effective relabelling effect on any second-moment $C_i^{\psi\phi}$ associated with vertical subfilter-scale fluxes of $\psi$ and $\phi$ and vertical variation of $\sigma_i$ |
| $D_i^{\psi}$                |                   | Rate of molecular dissipation of TKE ( $\psi = k$ ) or other second-moment quantity   |
| $S_i$                       |                   | Effective filter-scale entropy source in fluid $i$ due to TKE dissipation   |

## 2 | GOVERNING EQUATIONS

The flow is modelled by two fluids, with index “2” for updrafts and “1” for the environment. The governing equations are derived by conditional filtering of the compressible Euler equations (Thuburn *et al.*, 2018; 2022). The filter-scale state is assumed to be independent of  $x$  and  $y$ , so the equations simplify somewhat. The notation is summarized in Table 1. In the equations that follow,  $i = 1, 2$  and  $j = 3 - i$ .

### Volume fractions:

$$\sum_k \sigma_k = 1. \quad (1)$$

### Mass:

$$\frac{\partial m_i}{\partial t} + \frac{\partial F_i}{\partial z} = (\mathcal{M}_{ij} - \mathcal{M}_{ji}). \quad (2)$$

### Entropy:

$$\frac{\partial}{\partial t}(m_i \eta_i) + \frac{\partial}{\partial z}(F_i \eta_i + F_{SF}^{\eta_i}) = (\mathcal{M}_{ij} \hat{\eta}_{ij} - \mathcal{M}_{ji} \hat{\eta}_{ji}) + R_i^{\eta} + S_i. \quad (3)$$

### Water:

$$\frac{\partial}{\partial t}(m_i q_i) + \frac{\partial}{\partial z}(F_i q_i + F_{SF}^{q_i}) = (\mathcal{M}_{ij} \hat{q}_{ij} - \mathcal{M}_{ji} \hat{q}_{ji}) + R_i^q. \quad (4)$$

**Vertical velocity:**

$$\begin{aligned} \frac{\partial}{\partial t}(m_i w_i) + \frac{\partial}{\partial z}(F_i w_i + F_{\text{SF}}^{w_i}) + m_i \left( \frac{1}{\rho_i} \frac{\partial p}{\partial z} + \frac{\partial \Phi}{\partial z} \right) + \mathcal{P}_i \\ = (\mathcal{M}_{ij} \hat{w}_{ij} - \mathcal{M}_{ji} \hat{w}_{ji}) + R_i^w. \end{aligned} \quad (5)$$

For conservation of momentum  $\mathcal{P}_2 = -\mathcal{P}_1$ .

**Horizontal velocity:**

$$\begin{aligned} \frac{\partial}{\partial t}(m_i u_i) + \frac{\partial}{\partial z}(F_i u_i + F_{\text{SF}}^{u_i}) - f m_i (v_i - v_g) \\ = (\mathcal{M}_{ij} \hat{u}_{ij} - \mathcal{M}_{ji} \hat{u}_{ji}) + R_i^u, \end{aligned} \quad (6)$$

$$\begin{aligned} \frac{\partial}{\partial t}(m_i v_i) + \frac{\partial}{\partial z}(F_i v_i + F_{\text{SF}}^{v_i}) + f m_i (u_i - u_g) \\ = (\mathcal{M}_{ij} \hat{v}_{ij} - \mathcal{M}_{ji} \hat{v}_{ji}) + R_i^v. \end{aligned} \quad (7)$$

The entropy, water, and momentum component equations have been written in flux form to facilitate numerical conservation.

In principle, the horizontal momentum, Equations (6) and (7), should also include pressure drag terms—the horizontal analogues of the vertical drag  $\mathcal{P}_i$ —and there is evidence that these terms can be significant in sheared flows (e.g., Kershaw and Gregory, 1997; Romps, 2014, and references cited therein). However, these terms are neglected in the current model version.

**Turbulent kinetic energy (TKE):**

$$\begin{aligned} \frac{\partial}{\partial t}(m_i k_i) + \frac{\partial}{\partial z}(F_i k_i + T_i^{w u \cdot u} / 2) \\ = \frac{\sigma_i}{\rho_i} B_i^{\rho w} \frac{\partial p}{\partial z} + \sigma_i (w_2 - w_1) \mathcal{P}_2 - \mathbf{F}_{\text{SF}}^{u_i} \cdot \frac{\partial \mathbf{u}_i}{\partial z} \\ + \tilde{\mathcal{R}}_i^k + R_i^k - \mathcal{D}_i^k. \end{aligned} \quad (8)$$

The TKE equation is written in flux form to facilitate numerical conservation. Some terms involving pressure correlations have been assumed to vanish or to be negligible. The total dissipation of resolved kinetic energy by the pressure drag term is  $w_1 \mathcal{P}_1 + w_2 \mathcal{P}_2 = (w_2 - w_1) \mathcal{P}_2$ . It is not obvious how the resulting source of TKE should be partitioned between fluids 1 and 2, so we divide between the fluids in proportion to the volume fraction,  $\sigma_i$ .

**Scalar variances and covariances:**

$$0 = -2F_{\text{SF}}^{\eta_i} \frac{\partial \eta_i}{\partial z} + \mathcal{R}_i^{\eta\eta} + R_i^{\eta\eta} - \mathcal{D}_i^{\eta\eta}, \quad (9)$$

$$0 = -2F_{\text{SF}}^{q_i} \frac{\partial q_i}{\partial z} + \mathcal{R}_i^{qq} + R_i^{qq} - \mathcal{D}_i^{qq}, \quad (10)$$

$$0 = -F_{\text{SF}}^{\eta_i} \frac{\partial q_i}{\partial z} - F_{\text{SF}}^{q_i} \frac{\partial \eta_i}{\partial z} + \mathcal{R}_i^{\eta q} + R_i^{\eta q} - \mathcal{D}_i^{\eta q}. \quad (11)$$

In the variance and covariance equations, transience, advection, and third-order turbulent fluxes have been neglected, along with subfilter-scale correlations with sources.

**Subfilter-scale fluxes:**

$$0 = \sigma_i \tilde{B}_i^{p \partial \eta / \partial z} + \frac{\sigma_i}{\rho_i} B_i^{\rho \eta} \frac{\partial p}{\partial z} - \tilde{F}_{\text{SF}}^{w_i} \frac{\partial \eta_i}{\partial z}, \quad (12)$$

$$0 = \sigma_i \tilde{B}_i^{p \partial q / \partial z} + \frac{\sigma_i}{\rho_i} B_i^{\rho q} \frac{\partial p}{\partial z} - \tilde{F}_{\text{SF}}^{w_i} \frac{\partial q_i}{\partial z}, \quad (13)$$

$$0 = \sigma_i (\tilde{B}_i^{p \partial u / \partial z} + \tilde{B}_i^{p \partial w / \partial x}) - \tilde{F}_{\text{SF}}^{w_i} \frac{\partial u_i}{\partial z}, \quad (14)$$

$$0 = \sigma_i (\tilde{B}_i^{p \partial v / \partial z} + \tilde{B}_i^{p \partial w / \partial y}) - \tilde{F}_{\text{SF}}^{w_i} \frac{\partial v_i}{\partial z}. \quad (15)$$

In these flux equations, transience, advection, and third-order turbulent fluxes have been neglected, and also some terms involving subfilter-scale correlations with pressure fluctuations and with entropy sources.

Here,

$$\tilde{F}_{\text{SF}}^{w_i} = \frac{2}{3} m_i k_i \quad (16)$$

is an estimate for the subfilter-scale vertical flux of vertical momentum, approximated as two-thirds of the TKE. This should be a good approximation where the turbulence is nearly isotropic, but perhaps less so near the surface or boundary-layer top. The subfilter-scale vertical flux of vertical momentum used in the vertical momentum equation is calculated in a different way (Section 4.2).

The terms involving  $\partial p / \partial z$  in Equations (12) and (13) are buoyancy-correlation terms. Large-eddy simulation (LES) data (Efstathiou *et al.*, 2020) suggest they are important, for example, near the boundary-layer top for capturing upgradient fluxes associated with the fallback of overshooting thermals. However, these terms introduce complicated feedbacks in the numerical solver (Section 5) that compromise the solver stability. These terms will therefore not be included in this study or in the results presented in Part III (McIntyre *et al.*, 2022).

The relabelling terms in the TKE equation are given by

$$\begin{aligned} \tilde{\mathcal{R}}_i^k = \{ \mathcal{M}_{ij} (\hat{k}_{ij} + |\hat{\mathbf{u}}_{ij} - \mathbf{u}_i|^2 / 2) \\ - \mathcal{M}_{ji} (\hat{k}_{ji} + |\hat{\mathbf{u}}_{ji} - \mathbf{u}_i|^2 / 2) \} \end{aligned} \quad (17)$$

and the relabelling terms in the other second-moment equations are given by

$$\begin{aligned} \mathcal{R}_i^{ab} = & \{ \mathcal{M}_{ij} [\hat{C}_{ij}^{ab} - C_i^{ab} + (\hat{a}_{ij} - a_i)(\hat{b}_{ij} - b_i)] \\ & - \mathcal{M}_{ji} [\hat{C}_{ji}^{ab} - C_i^{ab} + (\hat{a}_{ji} - a_i)(\hat{b}_{ji} - b_i)] \}. \end{aligned} \quad (18)$$

The slightly different form arises because the TKE equation is written in flux form whereas the other second-moment equations are written in advective form. See Part I (Thuburn *et al.*, 2022) for a discussion of why it is necessary to write the second-moment equations in advective form before neglecting transience, advection, and flux terms.

The additional relabelling terms  $R_i^\psi$  and  $R_i^{\psi\phi}$  counteract the effect of vertical variations in  $\sigma_i$  on the divergence of the subfilter-scale flux and are discussed in detail in Part I (Thuburn *et al.*, 2022). In the first-moment equations they are given by

$$R_i^\psi = \frac{1}{\rho} \left( m_j \frac{\partial}{\partial z} F_{SF}^{\psi_j} - m_i \frac{\partial}{\partial z} F_{SF}^{\psi_i} \right). \quad (19)$$

In the TKE equation they are given by

$$\begin{aligned} R_i^k = & -\frac{1}{\rho} m_i \sum_k \mathbf{u}_k \cdot R_k^u \\ & + \frac{1}{\rho} \left( m_j \frac{\partial}{\partial z} T_i^{w\mathbf{u}\cdot\mathbf{u}} / 2 - m_i \frac{\partial}{\partial z} T_j^{w\mathbf{u}\cdot\mathbf{u}} / 2 \right), \end{aligned} \quad (20)$$

where  $R_j^u = (R_j^u, R_j^v, R_j^w)$ . Finally, in the other second-moment equations, for which the third-moment terms  $T$  are neglected, they are given by

$$R_i^{\psi\phi} = -\frac{1}{\rho} m_i \sum_k \psi_k R_k^\phi - \frac{1}{\rho} m_i \sum_k \phi_k R_k^\psi. \quad (21)$$

### 3 | THERMODYNAMICS

An equation of state is needed to relate  $p$ ,  $\rho$ ,  $\eta$ , and  $q$ . However, the calculation is non-trivial because, for some quantities, such as buoyancy, cloud fraction, and liquid water amount, subfilter-scale information must be taken into account.

To ensure thermodynamic consistency, the thermodynamics is formulated in terms of a Gibbs function (Thuburn, 2017a). Water may be in vapour or liquid form. Local thermodynamic equilibrium is assumed, so the relative humidity of the gaseous phase cannot exceed 1, and liquid is absent whenever the relative humidity is less

than 1. For brevity we will use the notation

$$p = P(\rho, \eta, q) \text{ or } \rho = \rho(p, \eta, q) \quad (22)$$

to refer to the solution of implicit equations

$$g_p(p, T, q) = 1/\rho; g_T(p, T, q) = -\eta, \quad (23)$$

where  $g(p, T, q)$  is the Gibbs function and the subscripts  $p$  and  $T$  indicate partial derivatives. When subfilter-scale information is not taken into account the equation of state is used in the form

$$p = P(\rho_i, \eta_i, q_i). \quad (24)$$

When subfilter-scale information is taken into account the equation of state is used in the form

$$\begin{aligned} \rho_i = & (\rho_g)_i + (q_1)_i \frac{\partial}{\partial q_1} (\rho - \rho_g) \\ = & \rho_g(p, \eta_i, q_i) + (q_1)_i \frac{\partial}{\partial q_1} (\rho - \rho_g). \end{aligned} \quad (25)$$

Here,  $\rho_g$  is the density that the air would have if all water remained in gaseous form, and  $(q_1)_i$  is the filter-scale-specific liquid water in fluid  $i$ .

Following Mellor (1977) and Sommeria and Dardorff (1977), subfilter-scale fluctuations in entropy and water are assumed to follow a joint Gaussian distribution and are assumed to be small enough to allow the equation of state to be linearized. Then,  $(q_1)_i$  is given by

$$\frac{(q_1)_i}{2\zeta_s} = \mathcal{Q} \mathcal{A}_i + \frac{1}{\sqrt{2\pi}} \exp\left(-\frac{\mathcal{Q}^2}{2}\right), \quad (26)$$

where

$$\mathcal{A}_i = \frac{1}{2} \left[ 1 + \operatorname{erf}\left(\frac{\mathcal{Q}}{\sqrt{2}}\right) \right] \quad (27)$$

is the cloud fraction,

$$\mathcal{Q} = \frac{\partial q_1}{\partial q} \Big|_\eta \frac{\Delta q}{2\zeta_s}, \quad (28)$$

$$\Delta q = q_i - Q_s(\eta_i) \quad (29)$$

is the supersaturation of the filter-scale state, and

$$4\zeta_s^2 = \left( \frac{\partial q_1}{\partial q} \Big|_\eta \right)^2 C_i^{qq} + 2 \frac{\partial q_1}{\partial q} \Big|_\eta \frac{\partial q_1}{\partial \eta} \Big|_q C_i^{\eta q} + \left( \frac{\partial q_1}{\partial \eta} \Big|_q \right)^2 C_i^{\eta\eta}. \quad (30)$$

The simplifications we make to the second-moment equations lead to an unrealistically strong correlation

between  $\eta$  and  $q$ ; therefore, for the purpose of the thermodynamics, we neglect the  $C_i^{\eta q}$  term in Equation (30).

## 4 | PARAMETERIZATIONS

### 4.1 | Turbulence time and length scales

A turbulence velocity scale is given by

$$U_i = \sqrt{2k_i}. \quad (31)$$

In each fluid, a master turbulence length scale  $L_i$  is defined as follows:<sup>1</sup>

$$\frac{1}{L_i} = \frac{1}{z} + \frac{1}{L_i^s}. \quad (32)$$

The length scale  $L_i^s$  is based on the distance a fluid parcel could travel against stratification,

$$\frac{1}{L_i^s} = \sqrt{\frac{\max(N_i^2, 0)}{k_i}}, \quad (33)$$

where

$$N_i = \sqrt{\frac{g}{\theta_i} \frac{\partial \theta_i}{\partial z}}$$

is the Brunt–Väisälä frequency for fluid  $i$ .  $L_i^s$  is then found by reducing the value of  $L_i^{s0}$  where necessary so that  $dL_i^s/dz$  does not exceed 1 in magnitude. Note that this modification introduces some non-local dependence in the turbulence length scale. A master turbulence time-scale is then defined in each fluid

$$\tau_i = L_i/U_i. \quad (34)$$

Also, a plume length scale is defined as

$$L_i^{\text{PLM}} = L_2^s. \quad (35)$$

Since we use a prognostic TKE while diagnosing other second moments, our governing equations resemble those of a level-2.5 Mellor–Yamada model (Mellor and Yamada, 1982). Several researchers (e.g. Helfand and Labraga, 1988; Janjić, 2001; Nakanishi, 2001) have discussed an important limitation of the level-2.5 model: all of the diagnosed second moments are related to the predicted

<sup>1</sup>We also experimented with length scale averaging of the form  $(1/L_i)^n = (1/z)^n + (1/L_i^s)^n$  for  $n > 1$ , but found that a similar effect on model behaviour could be achieved by tuning other parameters. An alternative “smooth minimum” function for obtaining the master turbulence length scale from a set of candidate length scales is given by Lopez-Gomez *et al.* (2020).

TKE by a certain system of equations; when turbulence is convectively driven and is growing towards its equilibrium intensity this system can become singular, leading to unphysical values of some quantities and even causing the model to “blow up”. When the scalar–buoyancy correlation terms are included our two-fluid model experiences essentially the same problem. Therefore, we expect that some mitigation, such as the reduction of certain turbulent time-scales (as suggested by Janjić, 2001), will be needed when buoyancy correlation terms are introduced in future versions of the model.

### 4.2 | Subfilter-scale fluxes

First consider the subfilter-scale scalar flux, Equations (12) and (13). Following Mellor and Yamada (1982), the pressure–scalar-gradient correlation terms are modelled as sink terms:

$$\begin{aligned} \sigma_i \bar{B}_i^{\rho \partial \eta / \partial z} &= -\frac{1}{\tau_i^{\text{sflx}}} m_i C_i^{w\eta}, \\ \sigma_i \bar{B}_i^{\rho \partial q / \partial z} &= -\frac{1}{\tau_i^{\text{sflx}}} m_i C_i^{wq}. \end{aligned} \quad (36)$$

The time-scale  $\tau_i^{\text{sflx}}$  appearing in these equations is related to the master time-scale by a tunable constant:  $\tau_i^{\text{sflx}} = 3A_2^{\text{MY}} \tau_i$ . The notation  $A_2^{\text{MY}}$  indicates that this parameter corresponds to the parameter  $A_2$  of Mellor and Yamada (1982), and similarly for  $A_1^{\text{MY}}$ ,  $B_2^{\text{MY}}$ , and  $B_2^{\text{MY}}$  later herein. The value chosen for  $A_2^{\text{MY}}$  will be discussed in Part III (McIntyre *et al.*, 2022).

Substituting Equation (36) into Equations (12) and (13) gives expressions for the subfilter-scale scalar fluxes

$$F_{\text{SF}}^{\phi_i} = m_i C_i^{w\phi} = -m_i K_i^s \frac{\partial \phi_i}{\partial z}, \quad (37)$$

where

$$m_i K_i^s = \tau_i^{\text{sflx}} \bar{F}_{\text{SF}}^{wi} = \frac{2}{3} \tau_i^{\text{sflx}} m_i k_i \quad (38)$$

defines the scalar eddy diffusivity  $K_i^s$ .

Next, consider the buoyancy–scalar correlation terms. Under the assumptions used in Section 3, it may be shown that

$$\begin{aligned} B_i^{\rho\phi} &= \left[ \frac{\partial \rho_g}{\partial \eta} \Big|_q + \mathcal{A}_i \frac{\partial q_1}{\partial \eta} \Big|_q \frac{\partial}{\partial q_1} (\rho - \rho_g) \right] B_i^{\eta\phi} \\ &+ \left[ \frac{\partial \rho_g}{\partial q} \Big|_\eta + \mathcal{A}_i \frac{\partial q_1}{\partial q} \Big|_\eta \frac{\partial}{\partial q_1} (\rho - \rho_g) \right] B_i^{q\phi} \\ &= (D_i^\eta B_i^{\eta\phi} + D_i^q B_i^{q\phi}) \\ &\approx (D_i^\eta C_i^{\eta\phi} + D_i^q C_i^{q\phi}), \end{aligned} \quad (39)$$

with  $\phi = q$  or  $\phi = \eta$ , where  $\mathcal{A}_i$  is the cloud fraction, and Equation (39) defines  $D_i^\eta$  and  $D_i^q$ . The buoyancy flux term in the TKE equation is computed by analogy with Equation (39):

$$\frac{\sigma_i B_i^{\rho w}}{\rho_i} \frac{\partial p}{\partial z} \approx \frac{1}{\rho_i^2} (D_i^\eta F_{SF}^{\eta_i} + D_i^q F_{SF}^{q_i}) \frac{\partial p}{\partial z}. \quad (40)$$

Next, consider the subfilter-scale vertical fluxes of  $u$  and  $v$ , Equations (14) and (15). Again following Mellor and Yamada (1982), the pressure–strain correlation terms are modelled as sink terms:

$$\begin{aligned} \sigma_i (\tilde{B}_i^{p \partial u / \partial z} + \tilde{B}_i^{p \partial w / \partial x}) &= -\frac{1}{\tau_i^{\text{uflx}}} m_i C_i^{wu}, \\ \sigma_i (\tilde{B}_i^{p \partial v / \partial z} + \tilde{B}_i^{p \partial w / \partial y}) &= -\frac{1}{\tau_i^{\text{uflx}}} m_i C_i^{wv}. \end{aligned} \quad (41)$$

The time-scale  $\tau_i^{\text{uflx}}$  appearing in these equations is related to the master time-scale by a tunable constant:  $\tau_i^{\text{uflx}} = 3A_1^{\text{MY}} \tau_i$ . The value chosen for  $A_1^{\text{MY}}$  will be discussed in Part III (McIntyre *et al.*, 2022).

Substituting in Equations (14) and (15) gives expressions for the subfilter-scale vertical fluxes of  $u$  and  $v$ :

$$\begin{aligned} F_{SF}^{u_i} &= m_i C_i^{wu} = -m_i K_i^u \frac{\partial u_i}{\partial z}, \\ F_{SF}^{v_i} &= m_i C_i^{wv} = -m_i K_i^u \frac{\partial v_i}{\partial z}, \end{aligned} \quad (42)$$

where  $K_i^u = \frac{2}{3} \tau_i^{\text{uflx}} k_i$  is the eddy diffusivity.

The subfilter-scale flux of  $w$  is parametrized as a down-gradient diffusion with the same eddy diffusivity as for other velocity components:

$$F_{SF}^{w_i} = -m_i K_i^u \frac{\partial w_i}{\partial z}. \quad (43)$$

The subfilter-scale flux of TKE is also parametrized as a downgradient diffusion with the same eddy diffusivity as for other fields:

$$T_i^{w \cdot u} / 2 = -m_i K_i^u \frac{\partial k_i}{\partial z}. \quad (44)$$

### 4.3 | Surface fluxes

The test cases discussed in Part III (McIntyre *et al.*, 2022) involve specified time series of surface sensible heat flux  $H^S$  and latent heat flux  $H^L$ . For use in our SCM, these are re-expressed as surface fluxes of mass, water, and entropy, with  $H^q = H^L / L_0$  and  $L_0 = 2.5 \times 10^6$ . The fraction of these

fluxes going into fluid 2 is given by

$$f_2 = \begin{cases} \sigma_2, & H^S \leq 0, \\ \max(0.4, \min(\sigma_2 + 0.1, 1)), & H^S > 0, \end{cases} \quad (45)$$

where here  $\sigma_2$  is taken at the lowest model level, and  $f_1 = 1 - f_2$ . This expression was arrived at by empirical tuning. It ensures that, when  $H^S > 0$ , fluid 2 tends to become buoyant.

For thermodynamic consistency, the surface moisture flux appears as a surface flux in the mass budget and the total water budget

$$F_i = f_i H^q, F_i^q = f_i q_i H^q \quad (46)$$

composed of pure water  $q_i = 1$ . The surface entropy flux is given by

$$F_i^\eta = f_i \left( \frac{H^S}{T_i} + (\eta_v)_i H^q \right), \quad (47)$$

where  $\eta_v$  is the entropy of water vapour, with  $(\eta_v)_i$  and  $T_i$  evaluated at the surface.

### 4.4 | Surface stress

The region between the surface and the lowest model level where  $u$  and  $v$  are stored (height  $z_1$ ) is assumed to be a constant-flux layer, implying the standard logarithmic profile of filter-scale winds. Rearranging for the friction velocity, and hence the surface stress, gives

$$(F_{SF}^{u_i}, F_{SF}^{v_i}) = -\frac{m_i k_0^2 |\mathbf{v}_i| (u_i, v_i)}{\{\ln[(z_1 + z_0)/z_0]\}^2}. \quad (48)$$

Here,  $k_0$  is the von Kármán constant,  $z_0$  is the roughness length (taken to be 0.1 m), and  $\mathbf{v}_i = (u_i, v_i)$  is the filter-scale horizontal velocity vector evaluated at height  $z_1$ .

### 4.5 | Vertical pressure drag

Based on Romps and Charn (2015), the vertical drag due to subfilter-scale pressure fluctuations is parametrized as

$$\mathcal{P}_2 = m_2 \frac{|w_2 - w_1| (w_2 - w_1)}{z_*}, \quad (49)$$

with  $\mathcal{P}_1 = -\mathcal{P}_2$  as required for momentum conservation (Thuburn *et al.*, 2018). Here, the thermal radius is assumed to be proportional to the boundary-layer depth  $z_*$ .  $z_*$  is defined to be the height at which a parcel lifted from the

surface with mean surface entropy and specific humidity

$$\eta_{00} = \frac{m_1 \eta_1 + m_2 \eta_2}{m_1 + m_2}, \quad q_{00} = \frac{m_1 q_1 + m_2 q_2}{m_1 + m_2}, \quad (50)$$

first becomes neutrally buoyant relative to fluid 1 (ignoring condensation). A minimum value of 50 m is permitted for  $z_*$ .

## 4.6 | Entropy source

TKE dissipated by molecular viscosity must be returned as internal energy and, hence, appears as a source in the entropy equation:

$$S_i = \frac{D_i^k}{T_i}. \quad (51)$$

## 4.7 | Molecular dissipation

Following Mellor and Yamada (1982), molecular dissipation of second moments is assumed to occur on a time-scale proportional to the master turbulence time-scale:

$$\begin{aligned} D_i^k &= 2m_i \frac{1}{\tau_i^{\text{kdis}}} k_i, & D_i^m &= 2m_i \frac{1}{\tau_i^{\text{sdis}}} C_i^m, \\ D_i^{\eta q} &= 2m_i \frac{1}{\tau_i^{\text{sdis}}} C_i^{\eta q}, & D_i^{qq} &= 2m_i \rho_i \frac{1}{\tau_i^{\text{sdis}}} C_i^{qq}. \end{aligned} \quad (52)$$

Here, the TKE dissipation time-scale  $\tau_i^{\text{kdis}}$  and the scalar variance dissipation time-scale  $\tau_i^{\text{sdis}}$  are related to the master time-scale by two tunable constants:  $\tau_i^{\text{kdis}} = B_1^{\text{MY}} \tau_i$  and  $\tau_i^{\text{sdis}} = B_2^{\text{MY}} \tau_i$ . The values chosen for  $B_1^{\text{MY}}$  and  $B_2^{\text{MY}}$  will be discussed in Part III (McIntyre *et al.*, 2022).

## 4.8 | Entrainment and detrainment

Several types of entrainment and detrainment are implemented to represent a variety of physical processes.

For each entrainment/detrainment process (identified by superscript PROC) we need to model the mean properties of the relabelled fluid. Mass flux and EDMF schemes often make the approximation  $\hat{\phi}_{ij} \approx \phi_j$ . However, entrained or detrained air can have properties that are systematically different from the source fluid mean; for example, detrainment of the least buoyant or lowest  $w$  air. In a crude attempt to capture such ‘‘sorting’’ effects, here, for each entrainment/detrainment scheme, the mean

properties of the relabelled air are modelled by an interpolation between updraft and environment. For a scalar variable  $\phi$ , the transferred fluid property of a specific transfer regime (here identified as PROC) is given by

$$\hat{\phi}_{ij}^{\text{PROC}} = b_{ij}^{\text{PROC}} \phi_j + (1 - b_{ij}^{\text{PROC}}) \phi_i, \quad (53)$$

with a constant coefficient  $b_{ij}^{\text{PROC}}$ .

For second-moment quantities, we take  $b_{ij}^{\text{PROC}} = 1$ , giving, for example,  $\hat{C}_{ij}^{ab} = C_j^{ab}$  and slightly simplifying Equation (18). For first-moment quantities, these  $b$ -coefficients are diagnosed with the help of LES data in Part III (McIntyre *et al.*, 2022).

### 4.8.1 | Instability entrainment

Fluid is relabelled from environment to updraft when the environment is statically unstable, at a rate proportional to the inverse of the instability time-scale.

$$\mathcal{M}_{21}^{\text{INS}} = \mathcal{F}^{\text{INS}} m_1 \sqrt{-\min(0, N_1^2)}, \quad (54)$$

where  $\mathcal{F}^{\text{INS}}$  is a tunable parameter controlling the rate of transfer. There is no corresponding instability detrainment:

$$\mathcal{M}_{12}^{\text{INS}} = 0. \quad (55)$$

### 4.8.2 | Mixing and relaxation to uniform state

This type of entrainment and detrainment relaxes the updraft volume fraction towards a reference profile and the updraft and environment properties towards each other. It serves two functions. One is to model the physical process of mixing between the updraft and the environment when the environment is turbulent. The other is a convenient modelling function to effectively remove the updraft when the updraft volume fraction is small. In both cases the formulation is the same, but the relaxation time-scale becomes very short when the updraft volume fraction is small. In a future model version it would be desirable to separate these two functions.

A reference updraft volume fraction  $\sigma_{2,0}$  is defined; here, it is taken to be  $10^{-3}$ , independent of  $z$ . Let  $\sigma_{1,0} = 1 - \sigma_{2,0}$ . A relaxation rate is defined as  $r^{\text{RLX}} = 1/\Delta t$ , where

$\Delta t$  is the time step. A turbulent mixing rate is defined as

$$r^{\text{TRB}} = \mathcal{F}^{\text{MIX}} \frac{\sqrt{k_2}}{L_i^{\text{PLM}}}, \quad (56)$$

where  $\mathcal{F}^{\text{MIX}}$  is a tunable coefficient controlling the rate of mixing (once again set in McIntyre *et al.*, 2022). The final entrainment–detrainment mixing rate  $r^{\text{MIX}}$  is obtained by interpolating between these two rates depending on the updraft volume fraction. A smooth quartic interpolation is used to aid solver convergence and reduce numerical noise:

$$\xi = \min(2, \max(1, \sigma_2/\sigma_{2,0})); \quad (57)$$

$$\zeta = (\xi - 2)^2 [1 - (\xi - 1)^2], \quad (58)$$

resulting in the total mixing rate

$$r^{\text{MIX}} = \zeta r^{\text{RLX}} + (1 - \zeta) r^{\text{TRB}}. \quad (59)$$

An additional bounding factor is also needed to prevent negative relabelling rates:

$$B_i = \min \left( 1, \max \left( 0, \frac{2m_i}{\rho} - \sigma_{i,0} \right) \right), \quad (60)$$

meaning the total relabelling rates are given by

$$\begin{aligned} \mathcal{M}_{21}^{\text{M}} &= r^{\text{MIX}} m_2 B_1; \\ \mathcal{M}_{12}^{\text{M}} &= r^{\text{MIX}} m_1 B_2. \end{aligned} \quad (61)$$

It is easily verified that, when the bounds in Equation (60) are not active, the mass tendencies due to mixing entrainment and detrainment are

$$\begin{aligned} \mathcal{M}_{12}^{\text{M}} - \mathcal{M}_{21}^{\text{M}} &= r^{\text{MIX}} (\sigma_{1,0} \rho - m_1), \\ \mathcal{M}_{21}^{\text{M}} - \mathcal{M}_{12}^{\text{M}} &= r^{\text{MIX}} (\sigma_{2,0} \rho - m_2); \end{aligned} \quad (62)$$

that is, relaxation to the reference volume fractions at the rate  $r^{\text{MIX}}$ . (The relaxation rate is modified slightly when the bounds are active.)

In the limit where  $\sigma_2 \gg \sigma_{2,0}$ , the mixing term reduces to  $\mathcal{M}_{ij}^{\text{MIX}} \approx \mathcal{F}^{\text{M}} m_i \sigma_j \sqrt{k_2}/L_i^{\text{PLM}}$ , which is similar to the turbulent entrainment rate used in Cohen *et al.* (2020), with some subtle differences:

- Cohen *et al.* (2020) use the TKE of the environment rather than the updraft. This is partly because they assume there is no TKE present within the updraft.  $\mathcal{M}_{ij}^{\text{MIX}}$  instead uses the TKE of fluid 2, which gives a

more representative description of the local turbulence where the mixing is occurring.

- Cohen *et al.* (2020) use a length scale equal to the maximum height of the plume.  $\mathcal{M}_{ij}^{\text{MIX}}$  instead uses a length scale ( $L_i^{\text{PLM}}$ ) based on lifting of air parcels against stratification. The length scale is therefore defined more locally.

The model includes the option to use different  $b_{ij}^{\text{MIX}}$  coefficients in the cloud layer (henceforth denoted by a different identifier,  $b_{ij}^{\text{MIC}}$ ) because of significant differences in the transferred properties in these regions (see Part III; McIntyre *et al.*, 2022). A smooth transition from boundary-layer values to cloud-layer values is achieved using a weighting based on the amount of liquid water present:

$$W^{\text{CLD}} = \frac{1}{2} \{1 + \tanh[f^{\text{CLD}}(q_{1,2} - 10^{-5})]\}, \quad (63)$$

where  $f^{\text{CLD}} = 2 \times 10^3$  is a constant. Hence, the relabelling rate is split into two parts (with different  $b$ -coefficients), one dominant in cloud-free air,

$$\begin{aligned} \mathcal{M}_{21}^{\text{MIX}} &= (1 - W^{\text{CLD}}) r^{\text{MIX}} m_2 B_1; \\ \mathcal{M}_{12}^{\text{MIX}} &= (1 - W^{\text{CLD}}) r^{\text{MIX}} m_1 B_2, \end{aligned} \quad (64)$$

and one dominant in cloudy air,

$$\begin{aligned} \mathcal{M}_{21}^{\text{MIC}} &= W^{\text{CLD}} r^{\text{MIX}} m_2 B_1; \\ \mathcal{M}_{12}^{\text{MIC}} &= W^{\text{CLD}} r^{\text{MIX}} m_1 B_2. \end{aligned} \quad (65)$$

### 4.8.3 | Forced detrainment

Where the updraft decelerates rapidly due to negative buoyancy at the boundary-layer top and cloud top there should be strong detrainment. Evidence from LES and from simulations at cloud-permitting resolutions (e.g., Fletcher and Bretherton, 2010) indicates that the detrained air is biased towards that with the smallest (or most negative)  $w$ , thus “sorting” the updraft air.

Some initial experiments were carried out in which the updraft  $w$  was assumed to have a Gaussian subfilter-scale probability density function and the rate at which mass was detrained was proportional to the fraction of that probability density function with  $w < 0$ . However, more robust results were obtained by making the rate at which mass is detrained proportional to the convergence rate of the updraft (a measure of its deceleration), similar to Weller

and McIntyre (2019):

$$\begin{aligned} r^{\text{FRC}} &= \min(1/\Delta t, \mathcal{F}^{\text{FRC}} \max(0, -\partial w_2/\partial z)); \\ \mathcal{M}_{12}^{\text{FRC}} &= r^{\text{FRC}} m_2, \end{aligned} \quad (66)$$

where  $\mathcal{F}^{\text{FRC}}$  controls the rate of detrainment. The bound on the detrainment rate only comes into play when  $-\partial w_2/\partial z$  becomes very large at the top of the updraft and there would otherwise be a danger of the numerical method creating negative mass in fluid 2.

There is no corresponding forced entrainment:

$$\mathcal{M}_{21}^{\text{FRC}} = 0. \quad (67)$$

#### 4.8.4 | Net entrainment and detrainment

The net entrainment and detrainment are obtained by combining the previously mentioned contributions:

$$\mathcal{M}_{ij} = \mathcal{M}_{ij}^{\text{INS}} + \mathcal{M}_{ij}^{\text{MIX}} + \mathcal{M}_{ij}^{\text{MIC}} + \mathcal{M}_{ij}^{\text{FRC}}. \quad (68)$$

The properties of the entrained or detrained air are given by the appropriate weighted-mean; for example:

$$\begin{aligned} \mathcal{M}_{ij} \hat{q}_{ij} &= \mathcal{M}_{ij}^{\text{INS}} \hat{q}_{ij}^{\text{INS}} + \mathcal{M}_{ij}^{\text{MIX}} \hat{q}_{ij}^{\text{MIX}} \\ &+ \mathcal{M}_{ij}^{\text{MIC}} \hat{q}_{ij}^{\text{MIC}} + \mathcal{M}_{ij}^{\text{FRC}} \hat{q}_{ij}^{\text{FRC}}. \end{aligned}$$

Our use of  $\mathcal{M}^{\text{INS}}$  only for entrainment into fluid 2 and of  $\mathcal{M}^{\text{FRC}}$  only for detrainment from fluid 2 reflects the up–down asymmetry of the atmospheric convective boundary layer. An argument could be made for applying a similar instability entrainment as a source for downdrafts forced, for example, by radiative cooling in stratocumulus or by evaporation of condensate in deep convection. However, we have not yet applied our model to such flows, and it might be necessary to introduce a third, “downdraft”, fluid type in order for it to work well. We have experimented with a forced detrainment of descending environmental air as it approaches the ground and decelerates. Although such a term was effective in two-fluid simulations of radiative–convective equilibrium and Rayleigh–Bénard convection (which did have up–down symmetry; Weller *et al.*, 2020; Shipley *et al.*, 2022), it did not work well in our tests for a shallow convection case.

Note that we do not decompose entrainment and detrainment into “dynamical” and “turbulent” components in the same way as de Rooy *et al.* (2013, eq. 11) or Cohen *et al.* (2020), where either dynamical entrainment or dynamical detrainment may be active, but not both, at any given location, and where the turbulent component

has zero net entrainment minus detrainment of mass. The parametrizations in Equations (64) and (65) generally have both entrainment and detrainment acting at the same time, and so would have both dynamical and turbulent components if we were to decompose them in this way.

## 4.9 | Fixers

We have attempted to avoid, as far as possible, the use of ad hoc “fixers”, but a small number are needed for model robustness:

- A minimum permitted kinetic energy per unit mass  $k_{\min}$  is defined. We have used  $k_{\min} = 10^{-4} \text{ J}\cdot\text{kg}^{-1}$ . The contribution to the TKE tendency from the buoyancy flux term is bounded such that the change in TKE over one time step from this term alone cannot make  $k_i < k_{\min}$ . This bound is needed to cope with situations where the TKE has not yet spun up but there might be an imposed downward heat flux, implying a TKE sink, at the surface (such as the start of the ARM case, discussed in Part III; McIntyre *et al.*, 2022). In addition, the quasi-Newton solver increments are bounded so that the updated TKE cannot be less than  $k_{\min}$ .
- The discretization of advection and diffusion can cause buoyancy to become negative at the model level immediately above the top of the updraft, in turn resulting in  $w_2 < 0$  there. This is unsatisfactory both from a physical and from a numerical point of view. There does not seem to be any straightforward modification to the discretization that can remove the problem. Therefore, a pragmatic fixer is used. After the solver iterations are completed, at any model level where  $w_2 < w_1$  the values of  $w_i$ ,  $\eta_i$ , and  $q_i$  are set to homogenized values:

$$\begin{aligned} w^{\text{hmg}} &= \frac{m_1 w_1 + m_2 w_2}{m_1 + m_2}; \\ \eta^{\text{hmg}} &= \frac{m_1 \eta_1 + m_2 \eta_2}{m_1 + m_2}; \\ q^{\text{hmg}} &= \frac{m_1 q_1 + m_2 q_2}{m_1 + m_2}. \end{aligned} \quad (70)$$

- Within the quasi-Newton solver (see later) the increments of total specific humidity are bounded to prevent the generation of negative total specific humidity.
- Within the quasi-Newton solver the increments of  $\eta$ -variance and  $q$ -variance are bounded so that the updated value is no less than 0.1 times the value at the previous iteration. Effectively, this ensures that variances remain non-negative.

## 5 | DISCRETIZATION

### 5.1 | Time discretization

The model uses a semi-implicit Eulerian discretization. If the (spatially discrete) model state is represented by  $\mathbf{X}$  and is governed by a set of prognostic and diagnostic equations

$$\frac{d\mathbf{X}}{dt} = \mathbf{M}(\mathbf{X}), \mathbf{N}(\mathbf{X}) = \mathbf{0}, \quad (71)$$

then the time discretization is given by an off-centred Crank–Nicolson scheme:

$$\mathbf{X}^{n+1} - \alpha \Delta t \mathbf{M}(\mathbf{X}^{n+1}) = \mathbf{X}^n + \beta \Delta t \mathbf{M}(\mathbf{X}^n), \mathbf{N}(\mathbf{X}^{n+1}) = \mathbf{0}, \quad (72)$$

where superscript  $n$  indicates the state at step  $n$  and  $\alpha$  is an off-centring parameter with  $\beta = 1 - \alpha$ . Our experiments have typically used  $\alpha = 0.55$ .

### 5.2 | Space discretization

We wish to use a staggered vertical grid—essentially a Charney–Phillips grid (Charney and Phillips, 1953)—with  $w$ ,  $\eta$ ,  $q$  stored at “ $w$ -levels”, and  $p$ ,  $\rho$ ,  $\sigma$ ,  $u$ , and  $v$  stored at “ $p$ -levels”. We will need to be able to transfer quantities between  $w$ -levels and  $p$ -levels and to formulate conservative budgets on both  $w$ -levels and  $p$ -levels in a consistent way. Appendix B describes the vertical averaging and difference operators used, along with some useful discrete product rule formulas. The need for vertical averaging is minimized by storing the second-moment quantities  $k$ ,  $C^{\eta\eta}$ ,  $C^{qq}$ , and  $C^{\eta q}$  at  $p$ -levels.

Equations (2) and (6–8) are evaluated at  $p$ -levels and predict the quantities  $m_\ell$ ,  $m_\ell u_\ell$ ,  $m_\ell v_\ell$ , and  $m_\ell k_\ell$  respectively for fluid  $i$ . Here, subscript  $\ell$  is the level index; the fluid index  $i$  has been suppressed for clarity. The vertical flux divergence in these equations is discretized using Equation (B12).

Equations (3–5) are evaluated at  $w$ -levels and predict the quantities  $\overline{m}_{\ell+1/2}^r \eta_{\ell+1/2}$ ,  $\overline{m}_{\ell+1/2}^r q_{\ell+1/2}$ , and  $\overline{m}_{\ell+1/2}^r w_{\ell+1/2}$  respectively for fluid  $i$ , where  $\overline{(\ )}^r$  indicates a conservative remapping from  $p$ - to  $w$ -levels. Again, subscript  $\ell$  is the level index and the fluid index  $i$  has been suppressed. The vertical flux divergence in these equations is discretized using Equation (B11).

The surface fluxes of mass, water, and entropy are specified at the bottom boundary  $\ell = 1/2$ , consistent with their respective budget equations and the  $p$ -level and  $w$ -level discrete divergence operators, Equations (B12) and (B11), at the lowest model level.

All advection terms are evaluated using the simplest first-order upwind (donor cell) scheme. First, the mass fluxes in Equation (2) are evaluated:

$$F_{\ell+1/2} = w_{\ell+1/2} m_{\ell+1/2}^u, \quad (73)$$

where

$$m_{\ell+1/2}^u = \begin{cases} m_\ell & \text{if } w_{\ell+1/2} > 0; \\ m_{\ell+1} & \text{otherwise.} \end{cases} \quad (74)$$

The fluxes of  $p$ -level quantities are evaluated using, for example,

$$(Fu)_{\ell+1/2} = F_{\ell+1/2} u_{\ell+1/2}^u, \quad (75)$$

where  $u_{\ell+1/2}^u$  is defined analogously to  $m_{\ell+1/2}^u$ , with the upwind direction taken from the sign of  $F_{\ell+1/2}$ . The fluxes of  $w$ -level quantities are evaluated using, for example,

$$(Fq)_\ell = \overline{F}_\ell^p q_\ell^u, \quad (76)$$

where  $\overline{(\ )}^p$  indicates a linear interpolation from  $w$ - to  $p$ -levels, and the upwind direction is taken from the sign of  $\overline{F}_\ell^p$ .

Vertical derivatives appear in a number of the governing equations. They are evaluated, where possible, using Equation (B11) or Equation (B12); in some cases a vertical average is also needed to return the result at the required levels.

- The vertical pressure gradient in Equation (5) is evaluated using Equation (B11). The vertical geopotential gradient is simply set to a constant value in the current implementation. The overall pressure gradient plus geopotential gradient term is evaluated as

$$\overline{m}_{\ell+1/2}^r \left( \frac{1}{\rho_{\ell+1/2}} \frac{\partial p}{\partial z} \Big|_{\ell+1/2} + g \right).$$

- The vertical derivatives of  $u$ ,  $v$ , and TKE used to compute their eddy-diffusive fluxes (Equations 42 and 44) are evaluated using Equation (B11).
- The vertical derivatives of  $\eta$  and  $q$  used to compute their eddy-diffusive fluxes, Equation (37) are evaluated using Equation (B12).
- The vertical pressure gradient appearing in the buoyancy flux generation of TKE, Equation (40), is evaluated using Equation (B11) with constant extrapolation to the top and bottom boundaries and then averaged using Equation (B9).

- For the shear generation term in the TKE equation, Equation (8), the contribution involving  $\partial w/\partial z$  is evaluated in a straightforward way using Equation (B12) for the vertical derivative. The contributions involving  $\partial u/\partial z$  and  $\partial v/\partial z$  are first evaluated using Equation (B11) and then averaged to the required levels; for example:

$$\left. -F_{SF}^u \frac{\partial u}{\partial z} \right|_{\ell}^s,$$

where  $\bar{(\ )}^s$  indicates a conservative remapping from  $w$ - to  $p$ -levels.

- The source of TKE due to pressure drag, Equation (8), is evaluated on  $w$ -levels and then mapped to  $p$ -levels using conservative averaging (Equation (B10)).
- The vertical derivatives of  $\eta$  and  $q$  in the source terms for variances and covariances (Equations 9–11) are evaluated in a straightforward way using Equation (B12).
- Eddy diffusivity coefficients for  $\eta$ ,  $q$ , and  $w$  are evaluated directly from TKE and the turbulent time-scale on  $p$ -levels. Eddy diffusivity coefficients for  $u$  and  $v$  and TKE are first evaluated on  $p$ -levels and then averaged to  $w$ -levels using Equation (B7) with linear extrapolation to the top and bottom boundaries.
- Mass relabelling rates  $\mathcal{M}$  are first evaluated on  $p$ -levels. Where needed on  $w$ -levels they are conservatively averaged using Equation (B8).
- The contributions to the TKE relabelling term  $\mathcal{R}_i^k$  (Equation (17)) from  $(\hat{u}_{ij} - u_i)^2$ ,  $(\hat{v}_{ij} - v_i)^2$ , and so on are evaluated straightforwardly on  $p$ -levels, whereas the contributions from  $(\hat{w}_{ij} - w_i)^2$  and so on are vertically averaged using Equation (B10). The contributions to the  $\eta$  and  $q$  variance and covariance relabelling terms involving  $(\hat{\eta}_{ij} - \eta_i)^2$  and so on are vertically averaged using Equation (B10).

The equation of state merits some detailed discussion. To capture accurately the coupling between buoyancy and vertical velocity, a key advantage of the Charney–Phillips grid, the equation of state must be used at both  $p$ -levels and at  $w$ -levels (Thuburn, 2017b).

On  $p$ -levels, the role of the equation of state is to capture the pressure fluctuations associated with density fluctuations; that is, the restoring force behind acoustic wave propagation:

$$p_{\ell} = P(\rho_{\ell}, \bar{\eta}_{\ell}^s, \bar{q}_{\ell}^s). \quad (77)$$

This equation provides the  $p$  that is used in computing vertical pressure gradients. The vertical averaging of  $\eta$  and  $q$  entails little loss of accuracy.

On  $w$ -levels, the role of the equation of state is to capture the density fluctuations associated with fluctuations in entropy and water; hence, the buoyancy

$$\rho_{\ell+1/2} = \rho(\bar{p}_{\ell+1/2}^w, \eta_{\ell+1/2}, q_{\ell+1/2}), \quad (78)$$

where  $\bar{(\ )}^w$  indicates a linear interpolation from  $p$ - to  $w$ -levels.

This equation provides the density used in the vertical pressure gradient term in Equation (5). Here, the vertical averaging of  $p$  entails little loss of accuracy. Because the equation of state is actually computed via a Gibbs function (Equation (23)), the model carries two temperature fields: one at  $p$ -levels and one at  $w$ -levels.

It is not crucial to take into account subfilter-scale information in the  $p$ -level equation of state to capture compressibility effects. However, subfilter-scale fluctuations in  $\eta$  and  $q$  can significantly affect the cloud cover and the amount of liquid water, and hence the buoyancy. Therefore,  $\rho_{\ell+1/2}$  is, in fact, calculated using Equation (25), with  $\rho_g$  calculated using filter-scale quantities:

$$(\rho_g)_{\ell+1/2} = \rho_g(\bar{p}_{\ell+1/2}^w, \eta_{\ell+1/2}, q_{\ell+1/2}), \quad (79)$$

and with conservative averaging of  $\sqrt{C^{\eta\eta}}$  and  $\sqrt{C^{qq}}$  to  $w$ -levels used to calculate  $\zeta_s$  and  $\mathcal{Q}$ , and hence cloud fraction and  $q_1$ .

### 5.3 | Solver: Overview

The time discretization, Equation (71), gives rise to a system of non-linear equations that implicitly determine the new state  $\mathbf{X}^{n+1}$ . A natural choice to solve this system is a Newton method. Let  $\mathbf{X}^{(l)}$  be an approximation to  $\mathbf{X}^{n+1}$  after  $l$  Newton iterations. For a first guess we take  $\mathbf{X}^{(0)} = \mathbf{X}^n$ . Then, after  $l$  iterations, the residuals are

$$\begin{aligned} \mathbf{R}_{\mathbf{M}}^{(l)} &= (\mathbf{X}^n + \beta \Delta t \mathbf{M}(\mathbf{X}^n)) - (\mathbf{X}^{(l)} - \alpha \Delta t \mathbf{M}(\mathbf{X}^{(l)})), \\ \mathbf{R}_{\mathbf{N}}^{(l)} &= -\mathbf{N}(\mathbf{X}^{(l)}), \end{aligned} \quad (80)$$

and the Newton update is given by

$$\mathbf{J}\mathbf{X}' = \mathbf{R}^{(l)}, \quad (81)$$

$$\mathbf{X}^{(l+1)} = \mathbf{X}^{(l)} + \mathbf{X}', \quad (82)$$

where

$$\mathbf{J} = \begin{pmatrix} \mathbf{I} - \alpha \Delta t \nabla_{\mathbf{X}} \mathbf{M} \\ \nabla_{\mathbf{X}} \mathbf{N} \end{pmatrix}, \mathbf{R}^{(l)} = \begin{pmatrix} \mathbf{R}_{\mathbf{M}}^{(l)} \\ \mathbf{R}_{\mathbf{N}}^{(l)} \end{pmatrix}. \quad (83)$$

Since we will make various approximations, the following method is more rightly called a quasi-Newton method. Solving Equation (81) with the full Jacobian  $J$  would be expensive. Non-local dependencies in the turbulent length scales and boundary-layer depth would introduce some long-range couplings that make the matrix less sparse. Moreover, deriving all the terms in the Jacobian matrix would be difficult and error prone and be challenging for code maintenance.<sup>2</sup> Use of the full Jacobian matrix would also make the method difficult to extend to three dimensions.

The Newton method should still give satisfactory convergence using an approximated Jacobian matrix provided the approximation captures the stiffest terms and the most important couplings. However, we do not want to simplify the linear system too far or we will run into the convergence problems seen by Thuburn *et al.* (2019). In this model version we make the following approximations. The linear system, Equation (81), is broken into a number of smaller uncoupled linear systems:

- A system for the increments to  $w_i, \eta_i, q_i, m_i$ , and  $p$ .
- A system for the increments to the second moments  $k_i, F_{SF}^{\eta_i}, F_{SF}^{q_i}, C_i^{\eta\eta}, C_i^{qq}$ , and  $C_i^{\eta q}$ ,
- Four uncoupled systems for  $u_1, u_2, v_1$ , and  $v_2$ .

For each of these linear systems, couplings may be included to variables at the same model level  $\ell$  (e.g.,  $m'_\ell$  to  $p'_\ell$ ), to variables half a grid level above and below (e.g.,  $m'_\ell$  to  $w'_{\ell \pm 1/2}$ ), and to the same variable one grid level above and below (e.g.,  $u_\ell$  to  $u_{\ell \pm 1}$ ). These relatively local couplings are sufficient to capture the stiffest phenomena represented by the model, including acoustic wave propagation, vertical eddy diffusion, and advection, as well as relabelling. Limiting the vertical range of couplings accounted for in this way keeps the linear systems to a manageable size. The pressure subsystem is a 19-diagonal system, the second-moment subsystem is a 25-diagonal subsystem, and each horizontal velocity subsystem is tri-diagonal. Consequently, the solver cost scales linearly with the number of model levels.

Finally, not all terms in the linearization within this limited height range are retained; only those terms thought to be stiffest and; therefore; most important. See the following subsections for details.

In an adiabatic single-fluid dynamical core, neglecting subfilter-scale terms and other “physics” terms, it is

usual to eliminate unknowns by hand and reduce the linear system to a standard Helmholtz problem for a single unknown field, such as the pressure increment. Such a reduction is also possible in the multi-fluid case and can accommodate relabelling terms, too, provided they are spatially local. However, the vertical coupling associated with eddy-diffusive subfilter-scale fluxes is strong and cannot be accommodated in this Helmholtz problem approach. Thuburn *et al.* (2019) used a partial reduction of the linear system, eliminating all unknowns except  $w'_1, w'_2$ , and  $p'$ . In the new model version described here, we eliminate only a small subset of variables by hand, namely the increments to  $\sigma_i$  and temperature; the resulting linear systems, as summarized earlier herein, are then solved numerically.

At each Newton iteration we solve the six linear subsystems summarized earlier herein and then increment all the model state variables. Some further details of the linearization are given in the following.

## 5.4 | Linearization: $w$ - $\eta$ - $q$ - $m$ - $p$ subsystem

The  $w$ - $\eta$ - $q$ - $m$ - $p$  subsystem comprises approximate linearizations of Equations 1–5. The linearized version of the equation of state (Equation (23)) at both  $p$ -levels and  $w$ -levels, along with

$$m'_i = \sigma_i \rho'_i + \sigma'_i \rho_i, \quad (84)$$

are used to eliminate  $T$  increments and  $\rho$  increments by hand.

The linearization of Equation (1) is

$$\sum_i \frac{m'_i}{\rho_i} - \frac{\sigma_i}{\rho_i^2} \left\{ \frac{\partial \rho}{\partial p} p' + \frac{\partial \rho}{\partial \eta} \eta'_i + \frac{\partial \rho}{\partial q} q'_i \right\} = R_{\sigma_i}^{(l)}, \quad (85)$$

where the residual  $R_{\sigma_i}^{(l)}$  includes an additional contribution that comes from the elimination of temperature increments—note that Equation (23) will not be exactly satisfied after  $l$  iterations.

The linearization of the mass conservation equation, Equation (2), is

$$m'_i + \alpha \Delta t \frac{\partial F'_i}{\partial z} - \alpha \Delta t \left( \mathcal{M}'_{ij} - \mathcal{M}'_{ji} \right) = R_{m_i}^{(l)}. \quad (86)$$

$\partial F'_i / \partial z$  at level  $\ell$  includes the effects of  $w'_i$  at levels  $\ell \pm 1/2$  and the effects of  $m'_i$  at levels  $\ell, \ell \pm 1$ . Currently, only

<sup>2</sup>Jacobian-free Newton–Krylov methods (e.g., Knoll and Keyes, 2004) provide an interesting alternative approach but still require preconditioning for rapid convergence.

an approximate linearization of  $\mathcal{M}_{ij}$  is implemented that accounts for its dependence on  $m_i$  and  $m_j$ :

$$\mathcal{M}'_{ij} \approx \sum_{\text{PROC}} \frac{\partial \mathcal{M}_{ij}^{\text{PROC}}}{\partial m_i} m'_i + \frac{\partial \mathcal{M}_{ij}^{\text{PROC}}}{\partial m_j} m'_j. \quad (87)$$

Although Equations (3–5) are written in flux form, their linearized transport terms include contributions from  $m'_i$  and  $w'_i$  from levels too far away to be included in the linear system, as already discussed herein. We can partly account for these terms by using Equation (86) to rewrite the linearized equations in quasi-advective form. For example, consider the linearization of the  $\eta$  equation, Equation (3):

$$\begin{aligned} & \overline{m}_i^r \eta'_i + \overline{m}'_i \eta_i + \alpha \Delta t \left[ \frac{\partial}{\partial z} (\overline{F}_i^p \eta^u_i) + \frac{\partial}{\partial z} (\overline{F}_i^p \eta^u_i) \right] \\ & + \dots \\ & + \alpha \Delta t (-\overline{\mathcal{M}}'_{ij} \hat{\eta}_{ij} - \overline{\mathcal{M}}_{ij} \hat{\eta}'_{ij} + \overline{\mathcal{M}}'_{ji} \hat{\eta}_{ji} + \overline{\mathcal{M}}_{ji} \hat{\eta}'_{ji}) = R_{\eta_i}^{(l)}; \end{aligned} \quad (88)$$

the others are analogous. At level  $\ell + 1/2$ , the transport term involving  $\overline{F}_i^p$  would contain contributions from  $w'_i$  at levels  $\ell - 1/2$ ,  $\ell + 1/2$ , and  $\ell + 3/2$  and from  $m'_i$  at levels  $\ell - 1$ ,  $\ell$ ,  $\ell + 1$ , and  $\ell + 2$ .

First, note that using the discrete product rule, Equation (B19),<sup>3</sup> that

$$\frac{\partial}{\partial z} (\overline{F}_i^p \eta^u_i) = \overline{F}_i^p \frac{\partial}{\partial z} (\eta^u_i) + \overline{\eta}^u_i \frac{\partial}{\partial z} (\overline{F}_i^p). \quad (89)$$

Then, subtracting  $\overline{\eta}^u_i$  times  $\overline{(\ )}$  of Equation (86) and using Equation (89) gives

$$\begin{aligned} & \overline{m}_i^r \eta'_i + \overline{m}'_i (\eta_i - \overline{\eta}^u_i) \\ & + \alpha \Delta t \left[ \frac{\partial}{\partial z} (\overline{F}_i^p \eta^u_i) + \overline{F}_i^p \frac{\partial}{\partial z} (\eta^u_i) \right] \\ & + \dots + \alpha \Delta t [-\overline{\mathcal{M}}'_{ij} (\hat{\eta}_{ij} - \overline{\eta}^u_i) - \overline{\mathcal{M}}_{ij} \hat{\eta}'_{ij} \\ & + \overline{\mathcal{M}}'_{ji} (\hat{\eta}_{ji} - \overline{\eta}^u_i) + \overline{\mathcal{M}}_{ji} \hat{\eta}'_{ji}] \\ & = R_{\eta_i}^{(l)} - \overline{\eta}^u_i R_{m_i}^{(l)}. \end{aligned} \quad (90)$$

The term  $\overline{F}_i^p$  still contains some contributions from  $w'$  and  $m'$  from levels beyond the allowed stencil. However, those contributions are no longer differentiated with respect to  $z$ , so neglecting them is expected to be less problematic. In practice, at level  $\ell + 1/2$  we retain the contributions involving  $w'_{\ell+1/2}$  and neglect contributions

involving  $w'_{\ell-1/2}$ ,  $w'_{\ell+3/2}$ ; we also neglect contributions from  $m'$  in this term, though some of them could, in principle, be retained.

The linearization of the properties of relabelled fluid is approximated as

$$\hat{\phi}'_{ij} \approx \sum_{\text{PROC}} \frac{\mathcal{M}_{ij}^{\text{PROC}}}{\mathcal{M}_{ij}} \hat{\phi}_{ij}^{\text{PROC}'}, \quad (91)$$

where

$$\hat{\phi}_{ij}^{\text{PROC}'} = b_{ij}^{\text{PROC}} \phi'_j + (1 - b_{ij}^{\text{PROC}}) \phi'_i. \quad (92)$$

The linearization of the subfilter-scale flux terms in Equations (3–5) accounts only for the eddy diffusion contribution. Moreover, increments to  $m$  and to  $K$  are neglected. For example:

$$\left( \frac{\partial F_{\text{SF}}^m}{\partial z} \right)' \approx \frac{\partial}{\partial z} \left( -m_i K_i^s \frac{\partial \eta'}{\partial z} \right). \quad (93)$$

The linearization of the additional relabelling terms such as  $R_i^m$  is neglected.

In Equation (5), the linearization of the pressure gradient terms is

$$\begin{aligned} & \left[ \overline{m}_i^r \left( \frac{1}{\rho_i} \frac{\partial p}{\partial z} + \frac{\partial \Phi}{\partial z} \right) \right]' = \overline{m}'_i \left( \frac{1}{\rho_i} \frac{\partial p}{\partial z} + \frac{\partial \Phi}{\partial z} \right) \\ & + \overline{m}_i^r \frac{1}{\rho_i} \frac{\partial p'}{\partial z} - \overline{m}_i^r \frac{1}{\rho_i^2} \frac{\partial p}{\partial z} \left( \frac{\partial \rho}{\partial p} \overline{p}' + \frac{\partial \rho}{\partial \eta} \eta'_i + \frac{\partial \rho}{\partial q} q'_i \right). \end{aligned} \quad (94)$$

The linearization of the drag term, Equation (49), is

$$\mathcal{P}'_2 = -\mathcal{P}'_1 \approx 2m_2 \frac{|w_2 - w_1| (w'_2 - w'_1)}{z_*}. \quad (95)$$

Having solved this subsystem, temperature increments at  $p$ -levels and at  $w$ -levels are found by back-substitution into the linearized version of the equation of state, Equation (23).

## 5.5 | Linearization: Second-moment subsystem

Scalar fluxes are diagnosed directly rather than regarded as state variables to be incremented in the Newton solver. Nevertheless, we need to make use of linearized versions of those equations in the second-moment subsystem. It is convenient, and also anticipates a possible future extension to a Mellor–Yamada level 3 scheme, to include the

<sup>3</sup>There might be some advantage in using Equation (B21) instead, but we have not pursued this.

linearized flux equations in the subsystem rather than eliminate the flux increments by hand.

Only couplings to second-moment increments are included; couplings to other increments are neglected.

$$m_i k'_i + \alpha \Delta t \frac{\partial}{\partial z} (F_i k'_i) - \alpha \Delta t \frac{\partial}{\partial z} \left( \overline{m}_i^r K_i^u \frac{\partial k'_i}{\partial z} \right) - \alpha \Delta t \frac{\partial \overline{p}}{\partial z} \left[ \frac{1}{\rho_i^2} \frac{\partial \rho}{\partial \eta} (F_{SF}^{\eta i})' + \frac{1}{\rho_i^2} \frac{\partial \rho}{\partial q} (F_{SF}^{qi})' \right] + \alpha \Delta t 2m_i \frac{1}{\tau_{i, \text{kdis}}} k'_i + \alpha \Delta t \mathcal{M}_{ji} k'_i = R_{k_i}^{(l)}; \quad (96)$$

$$(F_{SF}^{\eta i})' - m_i \frac{\partial \eta_i}{\partial z} \frac{\partial K_i^s}{\partial k_i} k'_i = 0; \quad (97)$$

$$(F_{SF}^{qi})' - m_i \frac{\partial q_i}{\partial z} \frac{\partial K_i^s}{\partial k_i} k'_i = 0. \quad (98)$$

The residuals in Equations (97) and (98) are set to zero because the subfilter-scale scalar flux equation, Equation (37), is satisfied exactly at each solver iteration.

$$\begin{aligned} \frac{m_i}{\tau_{i, \text{sdis}}} (C_i^{\eta \eta})' + \mathcal{M}_{ij} (C_i^{\eta \eta})' - \mathcal{M}_{ij} (C_j^{\eta \eta})' + 2(F_{SF}^{\eta i})' \frac{\partial \eta}{\partial z} &= R_{C_i^{\eta \eta}}^{(l)}; \\ \frac{m_i}{\tau_{i, \text{sdis}}} (C_i^{qq})' + \mathcal{M}_{ij} (C_i^{qq})' - \mathcal{M}_{ij} (C_j^{qq})' + 2(F_{SF}^{qi})' \frac{\partial q}{\partial z} &= R_{C_i^{qq}}^{(l)}; \\ \frac{m_i}{\tau_{i, \text{sdis}}} (C_i^{\eta q})' + \mathcal{M}_{ij} (C_i^{\eta q})' - \mathcal{M}_{ij} (C_j^{\eta q})' + (F_{SF}^{\eta i})' \frac{\partial q}{\partial z} + (F_{SF}^{qi})' \frac{\partial \eta}{\partial z} &= R_{C_i^{\eta q}}^{(l)}. \end{aligned} \quad (101)$$

## 5.6 | Linearization: $u$ and $v$ equations

As with the  $w$ -level scalars, the prognostic equations for  $u$  and  $v$  are written in flux form, but it is convenient to convert their linearizations to a quasi-advective form. Consider the linearized  $u$  equation; the  $v$ -equation is analogous.

$$m_i u'_i + m'_i u_i + \alpha \Delta t \left[ \frac{\partial}{\partial z} (F_i u'^u_i) + \frac{\partial}{\partial z} (F'_i u^u_i) \right] + \dots + \alpha \Delta t (-\mathcal{M}'_{ij} \hat{u}_{ij} - \mathcal{M}_{ij} \hat{u}'_{ij} + \mathcal{M}'_{ji} \hat{u}_{ji} + \mathcal{M}_{ji} \hat{u}'_{ji}) = R_{u_i}^{(l)}. \quad (102)$$

(At level  $\ell$ , the transport term involving  $F'_i$  would contain contributions from  $w'_i$  at levels  $\ell - 1/2$  and  $\ell + 1/2$  and from  $m'_i$  at levels  $\ell - 1$ ,  $\ell$ , and  $\ell + 1$ .)

Using the discrete product rule, Equation (B18), gives

$$\frac{\partial}{\partial z} (F'_i u^u_i) = \overline{F'_i}^s \frac{\partial}{\partial z} (u^u_i) + \overline{u^u_i}^p \frac{\partial}{\partial z} (F'_i). \quad (103)$$

Then, subtracting  $\overline{u^u_i}^p$  times Equation (86) and using Equation (103) gives

$$m_i u'_i + m'_i (u_i - \overline{u^u_i}^p) + \alpha \Delta t \left[ \frac{\partial}{\partial z} (F_i u'^u_i) + \overline{F'_i}^s \frac{\partial}{\partial z} (u^u_i) \right] + \dots + \alpha \Delta t [-\mathcal{M}'_{ij} (\hat{u}_{ij} - \overline{u^u_i}^p) - \mathcal{M}_{ij} \hat{u}'_{ij} + \mathcal{M}'_{ji} (\hat{u}_{ji} - \overline{u^u_i}^p) + \mathcal{M}_{ji} \hat{u}'_{ji}] = R_{u_i}^{(l)} - \overline{u^u_i}^p R_{m_i}^{(l)}. \quad (104)$$

In the  $u_i$  subsystem, increments to all variables except  $u_i$  are neglected. Thus, we omit the terms involving  $m'_i$ ,  $F'_i$ ,  $\mathcal{M}'_{ij}$ , and  $\mathcal{M}'_{ji}$ .

The linearized Coriolis terms are also omitted, since they do not involve  $u'_i$ . The linearized divergence of the subfilter-scale flux is approximated in the same way as for  $w$ -level scalars:

$$\left( \frac{\partial F_{SF}^{u_i}}{\partial z} \right)' \approx \frac{\partial}{\partial z} \left( -\overline{m}_i^r K_i^u \frac{\partial u'_i}{\partial z} \right), \quad (105)$$

except that now the surface stress must also be linearized:

$$(F_{SF}^{u_i})' \approx -\frac{m_i k_0^2 (|\mathbf{v}_i| + u_i^2 / |\mathbf{v}_i|)}{\{\ln[(z_1 + z_0)/z_0]\}^2} u'_i, \quad (106)$$

where  $\mathbf{v}_i$ ,  $u_i$ , and  $u'_i$  are evaluated at model level 1.

## 6 | NUMERICAL PERFORMANCE

We have described various significant changes to the two-fluid model described in Thuburn *et al.* (2019), with the aim of creating a more robust and versatile model that can be used for simulating shallow convection. In this section, the numerical performance of the two-fluid model is evaluated for the ARM case—a shallow convection test case involving transient growth and decay of the cloud field (full details of the implementation are given in Part III; McIntyre *et al.*, 2022).

Using four iterations of the quasi-Newton solver per time step, we are able to achieve a time step of 30 s with

80 vertical levels (resolution of  $\Delta z = 20$  m at the bottom of the domain;  $\Delta z = 110$  m at the top of the domain), which is a considerable improvement on the 6 s time step used in Thuburn *et al.* (2019)—although such a direct comparison is not completely justified given the use of a  $\Delta z = 20$  m uniform grid in Thuburn *et al.* (2019).

Doubling the number of solver iterations to eight makes only very small differences to the results, suggesting that solver convergence is adequate with four iterations. However, the maximum of the residuals (Equation (80)) typically decreases only by a factor of about half per iteration, suggesting that there is scope for improvement. The largest residuals occur in the middle of the simulation, when the surface fluxes are strongest and the cloud field most active.

The mass, water, and entropy budgets exert a strong control on the evolution of the boundary layer and clouds, so good model conservation properties are essential. Here, we evaluate the model's conservation properties by diagnosing budget discrepancies. For any property  $\psi$ ,

$$\text{Discrepancy} = \frac{\Psi(t) - \Psi(0) - \Psi_{\text{BUD}}(t)}{\Psi(0)}, \quad (107)$$

where  $\Psi(t)$  is the domain integrated sum of  $\psi$  at time  $t$ , and  $\Psi_{\text{BUD}}(t)$  is the total budgeted change due to surface fluxes and internal sources, integrated up until  $t$ . A discrepancy of order  $10^{-16}$  is indicative of a quantity that is conserved to within machine precision. The discrepancies for mass, entropy, water, and energy are presented in Figure 1 for the case of four solver iterations. The smallest discrepancies occur for the mass, which is conserved to

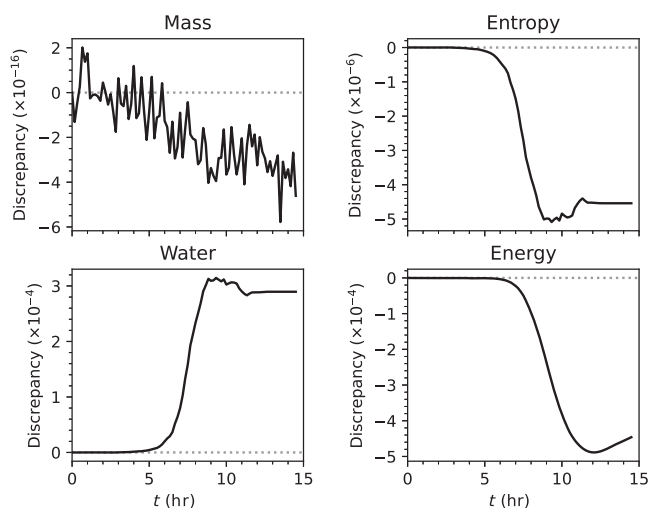


**FIGURE 1** The discrepancy of the mass, entropy, water, and energy relative to the expected changes due to the surface fluxes and internal sources. Each dataset has been normalized with respect to the initial total of each quantity

machine precision. The discrepancies for the total entropy and water grow most rapidly during the development phase of shallow cumulus convection. However, these discrepancies reduce significantly when the number of quasi-Newton iterations is increased, which implies that these discrepancies result from incomplete solver convergence. The discrepancy for the total energy does not reduce with a greater number of quasi-Newton iterations. This is expected, because the energy is not a prognostic variable; rather, it is instead diagnosed from the entropy and other model variables.

Another important numerical test is the convergence of the solution with increasing resolution. Using the ARM case once again, a high-resolution reference run was conducted with 640 vertical levels and a time step of 3.75 s. Four additional simulations were conducted using coarser resolutions, with the time step doubled for each halving of the number of levels. Figure 2 shows the relationship between the model errors and resolution for the vertical velocity, potential temperature, and moisture.

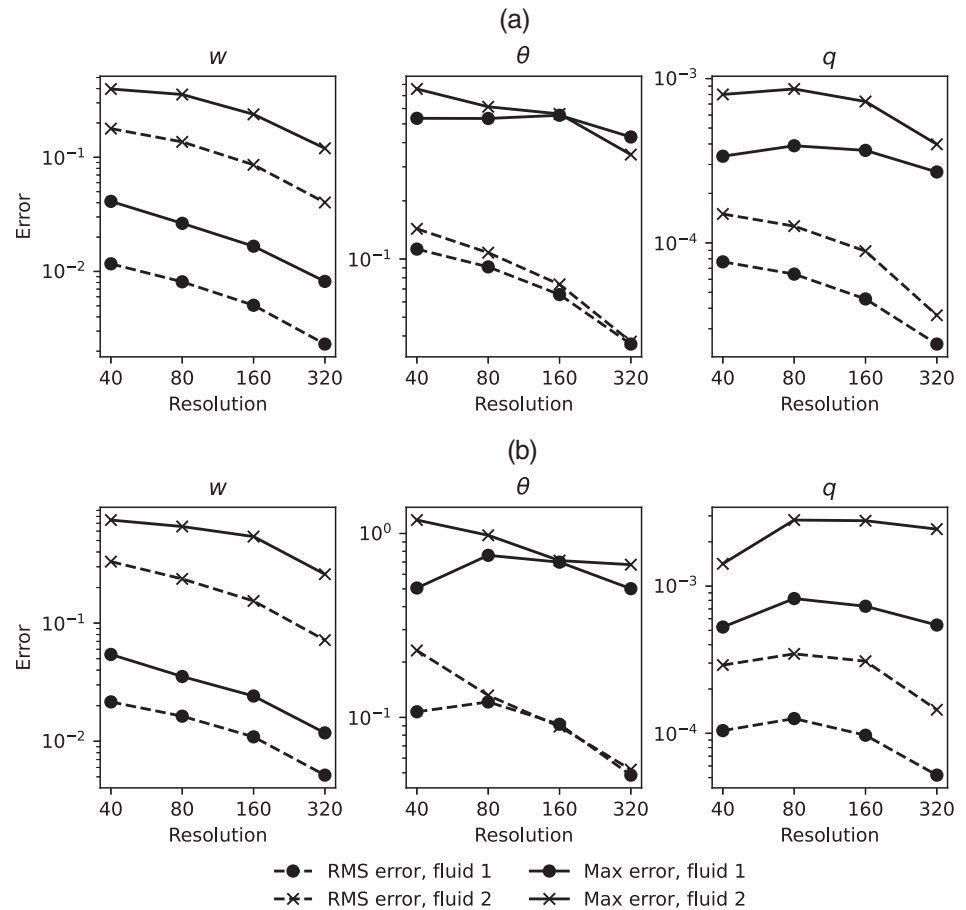
In the dry phase of the simulation (Figure 2a), the root-mean-square (RMS) errors reduce with each increase in resolution, as expected. All of the maximum errors occur at either the surface or the inversion layer, where gradients are at their sharpest, which the coarser simulations struggle to represent. The maximum errors for the fluid 2 vertical velocity and potential temperature reduce with each increase in resolution, which was not the case in Thuburn *et al.* (2019).

The convergence diagnostic shows a slightly more complicated relationship during the development phase of shallow convection (Figure 2b). As with the dry case, the RMS errors generally decrease with resolution. However, the errors for the coarsest resolution are relatively small for moisture and fluid 1 potential temperature. This is predominantly an artefact of an incorrect volume fraction at cloud base, as well as complicated feedbacks occurring at differing times.

## 7 | CONCLUSION

We have developed and improved the two-fluid SCM from Thuburn *et al.* (2019) to include moisture and higher-order moment quantities derived in Part I (Thuburn *et al.*, 2022). The governing equations differ from Thuburn *et al.* (2019) as the potential temperature has been replaced with entropy as a prognostic variable, and the TKE has been introduced as a prognostic variable. Equations for the scalar covariances and subfilter-scale fluxes are included, where the transience, advection, and third-order flux terms have been neglected. Subfilter-scale fluxes are approximated as downgradient eddy diffusive fluxes

**FIGURE 2** Errors of the two-fluid model versus resolution for the Atmospheric Radiation Measurement (ARM) case. Errors are relative to a high-resolution reference simulation with 640 cells in the vertical and a time step of 3.75 s. Data are shown for the vertical velocity (left), potential temperature (middle), and water (right) during the dry phase of the ARM case (top) and the development phase of shallow cumulus convection (bottom). Circles indicate fluid 1, whereas crosses indicate the fluid 2 data. Solid lines represent the maximum errors and dashed lines represent the root-mean-square (RMS) error. (a) Convergence 3 hr into ARM simulation. (b) Convergence 6 hr into ARM simulation



dependent on turbulent time and length scales. Scalar variances and covariances are diagnosed assuming local quasi-steady balances.

Three separate mechanisms are employed to represent entrainment and detrainment processes. An instability-based entrainment relabels unstable air to fluid 2 (which will mainly act near the surface), a forced detrainment removes air when fluid 2 is decelerating (and acts at the top of the boundary layer and cloud layer), and a TKE-dependent turbulent mixing term relaxes the volume fraction to a reference profile. The properties of the entrained and detrained air are controlled by a set of tunable parameters; the tuning of these parameters using LES diagnostics will be discussed in Part III (McIntyre *et al.*, 2022).

A semi-implicit Eulerian discretization was chosen, which offers improved stability over the semi-implicit semi-Lagrangian implementation of Thuburn *et al.* (2019) and longer time steps. The vertical discretization uses standard finite differences but exploits discrete product rules to improve conservation. The system is solved using a quasi-Newton method, where the first-order and second-order terms have been separated into independent linear systems to reduce complexity and computation

time. Despite these simplifications, the system adequately converges because the Jacobian contains all of the most important couplings, with roughly a halving of the maximum residuals with each quasi-Newton iteration. Mass is conserved in the two-fluid model to within machine precision, whereas the conservation of water and entropy is limited by the solver convergence but is adequate with four quasi-Newton iterations. Finally, the two-fluid model converges with increased resolution, confirming that the numerical methods are behaving as designed.

The two-fluid model presented in this article will be tested for two case studies of shallow cumulus convection in Part III (McIntyre *et al.*, 2022).

## AUTHOR CONTRIBUTIONS

**John Thuburn:** conceptualization; data curation; formal analysis; funding acquisition; investigation; methodology; project administration; software; validation; writing – original draft. **Georgios A. Efstathiou:** conceptualization; investigation; methodology; project administration; software; validation; writing – review and editing. **William A. McIntyre:** data curation; formal analysis; investigation; methodology; project administration;

software; validation; visualization; writing – review and editing.

## ACKNOWLEDGEMENTS

This work was funded by the Natural Environment Research Council under grants NE/N013123/1 and NE/T003863/1 as part of the ParaCon programme, as well as by the Weather and Climate Science for Service Partnership Southeast Asia under grant SEA21\_2.10.

We are grateful to Dr Yair Cohen and an anonymous reviewer for their constructive comments. We also thank Professor Hilary Weller for her careful reading and valuable feedback on an earlier version.

Simulations with the two-fluid SCM were conducted using MultiFluidSCM ([github.com/MultiFluidSCM](https://github.com/MultiFluidSCM)).

## ORCID

John Thuburn  <https://orcid.org/0000-0002-4598-546X>

Georgios A. Efstathiou  <https://orcid.org/0000-0003-3469-8729>

William A. McIntyre  <https://orcid.org/0000-0002-2715-9842>

## REFERENCES

- Charney, J.G. and Phillips, N.A. (1953) Numerical integration of the quasi-geostrophic equations for barotropic and simple baroclinic flow. *Journal of Meteorology*, 10, 71–99.
- Cohen, Y., Lopez-Gomez, I., Jaruga, A., He, J., Kaul, C.M. and Schneider, T. (2020) Unified entrainment and detrainment closures for extended eddy-diffusivity mass-flux schemes. *Journal of Advances in Modeling Earth Systems*, 12, e2020MS002162.
- de Rooy, W.C., Bechtold, P., Frölich, K., Hohenegger, C., Jonker, H., Mironov, D., Siebesma, A.P., Teixeira, J. and Yano, J.-I. (2013) Entrainment and detrainment in cumulus convection: an overview. *Quarterly Journal of the Royal Meteorological Society*, 139, 1–19.
- Efstathiou, G.A., Thuburn, J. and Beare, R.J. (2020) Diagnosing coherent structures in the convective boundary layer by optimising their vertical turbulent scalar transfer. *Boundary-Layer Meteorology*, 174, 119–144.
- Fletcher, J.K. and Bretherton, C.S. (2010) Evaluating boundary layer-based mass flux closures using cloud-resolving model simulations of deep convection. *Journal of the Atmospheric Sciences*, 67, 2212–2225.
- Helfand, H.M. and Labraga, J.C. (1988) Design of a nonsingular level 2.5 second-order closure model for the prediction of atmospheric turbulence. *Journal of the Atmospheric Sciences*, 45, 113–132.
- Janjić, C. I. (2001) *Nonsingular implementation of the Mellor–Yamada level 2.5 scheme in the NCEP Meso model*. National Centers for Environmental Prediction. Office Note No. 437.
- Kershaw, R. and Gregory, D. (1997) Parametrization of momentum transport by convection. I: theory and cloud modelling results. *Quarterly Journal of the Royal Meteorological Society*, 123, 1133–1151.
- Knoll, D.A. and Keyes, D.E. (2004) Jacobian-free Newton–Krylov methods: a survey of approaches and applications. *Journal of Computational Physics*, 193, 357–397.
- Lopez-Gomez, I., Cohen, Y., He, J., Jaruga, A. and Schneider, T. (2020) A generalized mixing length closure for eddy-diffusivity mass-flux schemes of turbulence and convection. *Journal of Advances in Modeling Earth Systems*, 12, e2020MS00216.
- McIntyre, W.A., Efstathiou, G.A. and Thuburn, J. (2022) A two-fluid single-column model of turbulent shallow convection, part III: results and parameter sensitivity. *Quarterly Journal of the Royal Meteorological Society*. Submitted.
- McIntyre, W.A., Weller, H. and Holloway, C.E. (2020) Numerical methods for entrainment and detrainment in the multi-fluid Euler equations for convection. *Quarterly Journal of the Royal Meteorological Society*, 146, 1106–1120.
- Mellor, G.L. (1977) The Gaussian cloud model relations. *Journal of the Atmospheric Sciences*, 34, 356–358.
- Mellor, G.L. and Yamada, T. (1982) Development of a turbulence closure model for geophysical fluid problem. *Reviews of Geophysics and Space Physics*, 20, 851–875.
- Nakanishi, M. (2001) Improvement of the Mellor–Yamada turbulence closure model based on large-eddy simulation data. *Boundary-Layer Meteorology*, 99, 349–978.
- Romps, D.M. (2014) Rayleigh damping in the free troposphere. *Journal of the Atmospheric Sciences*, 71, 553–565.
- Romps, D.M. and Charn, A.B. (2015) Sticky thermals: evidence for a dominant balance between buoyancy and drag in cloud updrafts. *Journal of the Atmospheric Sciences*, 72, 2890–2901.
- Shipley, D., Weller, H., Clark, P.A. and McIntyre, W.A. (2022) Two-fluid single-column modelling of Rayleigh–Bénard convection as a step towards multi-fluid modelling of atmospheric convection. *Quarterly Journal of the Royal Meteorological Society*, 148, 351–377.
- Sommeria, J. and Deardorff, J.W. (1977) Subgrid-scale condensation in models of nonprecipitating clouds. *Journal of the Atmospheric Sciences*, 34, 344–355.
- Tan, Z., Kaul, C.M., Pressel, K.G., Cohen, Y., Schneider, T. and Teixeira, J. (2018) An extended eddy-diffusivity mass-flux scheme for unified representation of subgrid-scale turbulence and convection. *Journal of Advances in Modeling Earth Systems*, 10, 770–800.
- Thuburn, J. (2017a) Use of the Gibbs thermodynamic potential to express the equation of state in atmospheric models. *Quarterly Journal of the Royal Meteorological Society*, 143, 1185–1196.
- Thuburn, J. (2017b) Vertical discretizations giving optimal representation of normal modes: general equations of state. *Quarterly Journal of the Royal Meteorological Society*, 143, 1714–1720.
- Thuburn, J., Efstathiou, G.A. and Beare, R.J. (2019) A two-fluid single-column model of the dry, shear-free, convective boundary layer. *Quarterly Journal of the Royal Meteorological Society*, 145, 1535–1550.
- Thuburn, J., Efstathiou, G.A. and McIntyre, W.A. (2022) A two-fluid single-column model of turbulent shallow convection, part I: turbulence equations in the multi-fluid framework. *Quarterly Journal of the Royal Meteorological Society*. Submitted.
- Thuburn, J. and Vallis, G.K. (2018) Properties of the conditionally filtered equations: conservation, normal modes, and variational formulation. *Quarterly Journal of the Royal Meteorological Society*, 144, 1555–1571.

- Thuburn, J., Weller, H., Vallis, G.K., Beare, R.J. and Whittall, M. (2018) A framework for convection and boundary layer parameterization derived from conditional filtering. *Journal of the Atmospheric Sciences*, 75, 965–981.
- Weller, H., McIntyre, W. and Shipley, D. (2020) Multifluids for representing subgrid-scale convection. *Journal of Advances in Modeling Earth Systems*, 12, e2019MS001966.
- Weller, H. and McIntyre, W.A. (2019) Numerical solution of the conditionally averaged equations for representing net mass flux due to convection. *Quarterly Journal of the Royal Meteorological Society*, 145, 1337–1353.

**How to cite this article:** Thuburn, J., Efstathiou, G.A. & McIntyre, W.A. (2022) A two-fluid single-column model of turbulent shallow convection. Part II: Single-column model formulation and numerics. *Quarterly Journal of the Royal Meteorological Society*, 1–22. Available from: <https://doi.org/10.1002/qj.4361>

## APPENDIX A. STABILITY ANALYSIS: CONTINUOUS EQUATIONS AND SEMI-IMPLICIT EULERIAN AND SEMI-LAGRANGIAN SCHEMES

For tractability, consider a simplified one-dimensional two-fluid system with uniform entropy and zero moisture and neglect all subfilter-scale and relabelling terms except for an eddy diffusion term in the vertical velocity equation:

$$\frac{\partial}{\partial t}(\sigma_i \rho_i) + \frac{\partial}{\partial z}(\sigma_i \rho_i w_i) = 0, \quad (\text{A1})$$

$$\frac{D_i}{Dt} w_i + \frac{1}{\rho_i} \frac{\partial p}{\partial z} = \frac{1}{\rho_i} \frac{\partial}{\partial z} \left( \rho_i K \frac{\partial w_i}{\partial z} \right). \quad (\text{A2})$$

Linearize about a basic state (independent of  $z$  and  $t$ ) with  $\sigma_i = \sigma_i^0$ ,  $\rho_i = \rho^0$ ,  $w_i = W_i$ , and  $K$  constant. Assume

$$\frac{p'}{c^2} = \rho'_i = \sum_i (\sigma_i \rho_i)', \quad (\text{A3})$$

where  $c$  is a constant sound speed, and note

$$\sum_i \sigma'_i = 0. \quad (\text{A4})$$

## Continuous equations

For the continuous equations, the linearized system is

$$\rho^0 \frac{\partial \sigma'_i}{\partial t} + \sigma_i^0 \frac{\partial \rho'_i}{\partial t} + \sigma_i^0 \rho^0 \frac{\partial w'_i}{\partial z} + \sigma_i^0 W_i \frac{\partial \rho'_i}{\partial z} + \rho^0 W_i \frac{\partial \sigma'_i}{\partial z} = 0, \quad (\text{A5})$$

$$\frac{\partial w'_i}{\partial t} + W_i \frac{\partial w'_i}{\partial z} + \frac{1}{\rho^0} \frac{\partial p'}{\partial z} = K \frac{\partial^2}{\partial z^2} w'_i, \quad (\text{A6})$$

together with Equations A3 and A4.

Seeking solutions proportional to  $\exp\{i(mz - \omega t)\}$  and eliminating unknowns leads to the dispersion relation

$$\frac{1}{m^2 c^2} = - \sum_i \left[ \frac{\sigma_i^0}{(-i\omega + imW_i)(-i\omega + imW_i + m^2 K)} \right]. \quad (\text{A7})$$

In the limit of large  $c$ , two of the roots for  $\omega$  correspond to acoustic modes with frequency close to  $\pm mc$ , with the next order correction describing a Doppler shift by the mean flow and a damping by the eddy diffusion:

$$\omega \approx \pm mc + m(\sigma_1^0 W_1 + \sigma_2^0 W_2) - \frac{1}{2} im^2 K. \quad (\text{A8})$$

For the other two roots,

$$\omega \approx m(\sigma_1^0 W_1 + \sigma_2^0 W_2) - \frac{1}{2} im^2 K \pm \left[ -\sigma_1^0 \sigma_2^0 m^2 (W_2 - W_1)^2 - \left( \frac{m^2 K}{2} \right)^2 \right]^{1/2}. \quad (\text{A9})$$

When  $K = 0$ , this result agrees with the incompressible analysis of Thuburn *et al.* (2019, app. A) describing the Kelvin–Helmholtz-like instability of the two-fluid equations. One of the roots here corresponds to instability for any value of  $K$ , though the growth rate decreases as  $K$  increases. Thus, vertical diffusion of  $w$ , on its own, cannot completely suppress the instability.

## Semi-implicit Eulerian discretization

For an off-centred Crank–Nicolson time discretization with off-centring parameters  $\alpha$  and  $\beta = 1 - \alpha$ , the amplification factor  $A$  satisfies

$$\frac{A - 1}{\alpha A + \beta} = -i\omega \Delta t, \quad (\text{A10})$$

where  $\omega$  is the continuous frequency and  $\Delta t$  is the time step. Hence:

$$A = \frac{1 - i\omega \beta \Delta t}{1 + i\omega \alpha \Delta t}. \quad (\text{A11})$$

It is easily verified that  $|A| \leq 1$  for the damped case  $\omega_i \leq 0$  provided  $\alpha \geq 1/2$ .

### Semi-implicit semi-Lagrangian discretization

Writing Equation (A1) in advective form, discretizing Equations A1 and A2 with a semi-implicit semi-Lagrangian scheme, and linearizing gives

$$\begin{aligned} & \left( \rho^0 \sigma'_i + \sigma_i^0 \frac{p'}{c^2} + \alpha \Delta t \sigma_i^0 \rho^0 \frac{\partial w'_i}{\partial z} \right)^{n+1} \\ &= \left( \rho^0 \sigma'_i + \sigma_i^0 \frac{p'}{c^2} - \beta \Delta t \sigma_i^0 \rho^0 \frac{\partial w'_i}{\partial z} \right)_{D_i}^n, \end{aligned} \quad (\text{A12})$$

$$\begin{aligned} & \left[ w'_i + \alpha \Delta t \left( \frac{1}{\rho^0} \frac{\partial p'}{\partial z} - K \frac{\partial^2 w'_i}{\partial z^2} \right) \right]^{n+1} \\ &= \left[ w'_i - \beta \Delta t \left( \frac{1}{\rho^0} \frac{\partial p'}{\partial z} - K \frac{\partial^2 w'_i}{\partial z^2} \right) \right]_{D_i}^n, \end{aligned} \quad (\text{A13})$$

where superscripts  $n$  and  $n+1$  indicate the time step number and subscript  $D_i$  indicates a quantity evaluated at a departure point computed using velocity  $W_i$ . Equation (A3) has been used to eliminate density perturbations.

Seek solutions proportional to  $A^n \exp(imz)$  and let

$$E_i = \exp(-imW_i \Delta t) \quad (\text{A14})$$

be the advective Doppler shift factor assuming perfect interpolation to departure points. Eliminating unknowns then leaves the discrete dispersion relation

$$\frac{1}{m^2 c^2} = - \sum_i \left[ \frac{(\alpha \Delta t A + \beta \Delta t E_i)^2 \sigma_i^0}{(A - E_i)(A q^+ - E_i q^-)} \right], \quad (\text{A15})$$

where  $q^+ = 1 + \alpha \Delta t m^2 K$  and  $q^- = 1 - \beta \Delta t m^2 K$ .

Even making simplifying assumptions such as  $1/c^2 = 0$  and  $K = 0$ , it does not appear tractable to solve analytically for  $A$ . However, numerical solution of the discrete dispersion relation for typical parameter values shows instability can easily occur, even with off-centring and strong diffusion.

## APPENDIX B. DISCRETE AVERAGING AND PRODUCT RULES

Consider a vertically staggered grid with  $p$ -levels indexed by integers interleaved with  $w$ -levels indexed by integers plus  $1/2$  (Figure B1). Level  $1/2$  coincides with

the domain bottom boundary, and level  $N + 1/2$  coincides with the model top.

Let

$$\Delta z_\ell = z_{\ell+1/2} - z_{\ell-1/2}, \ell = 1, \dots, N. \quad (\text{B1})$$

Let

$$\begin{aligned} & \Delta z_{\ell+1/2} = z_{\ell+1} - z_\ell, \ell = 1, \dots, N-1, \\ & \text{with } \Delta z_{1/2} = z_1 - z_{1/2}, \Delta z_{N+1/2} = z_{N+1/2} - z_N. \end{aligned} \quad (\text{B2})$$

Define the following sets of coefficients in terms of the locations of the model levels:

$$\begin{aligned} a_\ell &= \frac{z_\ell - z_{\ell-1/2}}{\Delta z_\ell}, b_\ell = \frac{z_{\ell+1/2} - z_\ell}{\Delta z_\ell} \\ &= 1 - a_\ell, \ell = 1, \dots, N; \\ a_{\ell+1/2} &= \frac{z_{\ell+1/2} - z_\ell}{\Delta z_{\ell+1/2}}, b_{\ell+1/2} = \frac{z_{\ell+1} - z_{\ell+1/2}}{\Delta z_{\ell+1/2}} = 1 - a_{\ell+1/2}, \\ & \ell = 1, \dots, N-1, \end{aligned}$$

$$\text{with } a_{1/2} = 1, b_{1/2} = 0, a_{N+1/2} = 0, b_{N+1/2} = 1; \quad (\text{B4})$$

$$A_\ell = b_\ell, B_\ell = a_\ell, \ell = 1, \dots, N; \quad (\text{B5})$$

$$A_{\ell+1/2} = b_{\ell+1/2}, B_{\ell+1/2} = a_{\ell+1/2},$$

$$\ell = 1, \dots, N-1,$$

$$\text{with } A_{1/2} = 1, B_{1/2} = 0, A_{N+1/2} = 0, B_{N+1/2} = 1. \quad (\text{B6})$$

Let  $e_\ell$  and  $f_\ell$  be two variables that reside at  $p$ -levels and let  $g_{\ell+1/2}$  and  $h_{\ell+1/2}$  be two variables that reside at  $w$ -levels. Then we can define the following four averaging operators.

**Linear interpolation to  $w$ -levels with constant extrapolation at boundaries:**

$$\bar{f}_{\ell+1/2}^w = a_{\ell+1/2} f_{\ell+1} + b_{\ell+1/2} f_\ell. \quad (\text{B7})$$

**Depth-weighted remapping to  $w$ -levels, or projection of a piecewise constant field to a new piecewise constant field:**

$$\bar{f}_{\ell+1/2}^r = A_{\ell+1/2} f_{\ell+1} + B_{\ell+1/2} f_\ell. \quad (\text{B8})$$

**Linear interpolation to  $p$ -levels:**

$$\bar{g}_\ell^p = a_\ell g_{\ell+1/2} + b_\ell g_{\ell-1/2}. \quad (\text{B9})$$

**Depth-weighted remapping to  $p$ -levels, or projection of a piecewise constant field to a new piecewise constant field:**

$$\bar{g}_\ell^s = A_\ell g_{\ell+1/2} + B_\ell g_{\ell-1/2}. \quad (\text{B10})$$

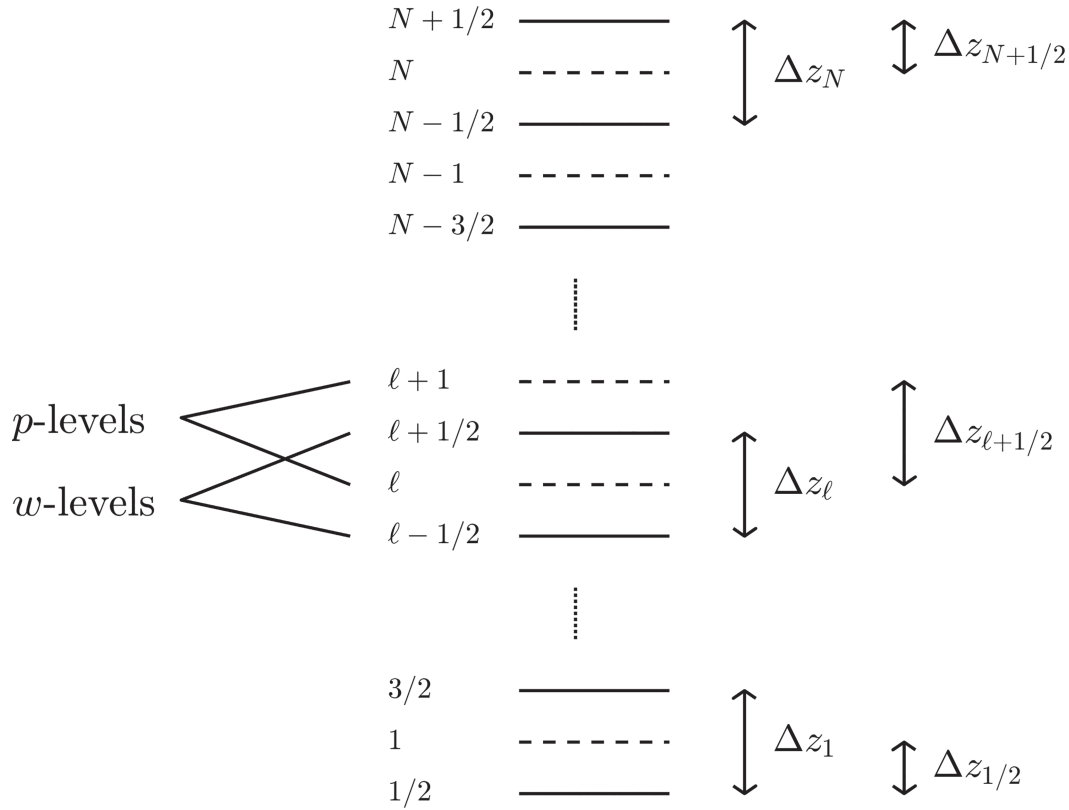


**FIGURE B1** Schematic showing the vertically staggered grid and the indexing of the model levels

Also define the natural finite-difference derivative operators:

$$\left. \frac{\partial f}{\partial z} \right|_{\ell+1/2} = \frac{f_{\ell+1} - f_{\ell}}{\Delta z_{\ell+1/2}}; \tag{B11}$$

$$\left. \frac{\partial g}{\partial z} \right|_{\ell} = \frac{g_{\ell+1/2} - g_{\ell-1/2}}{\Delta z_{\ell}}. \tag{B12}$$

The expression in Equation (B11) remains valid at  $\ell = 0$  and  $\ell = N$  provided  $f_0$  and  $f_{N+1}$  are interpreted as values at the bottom and top boundaries respectively.

The following properties are then easily verified.

(i)  $\bar{()^r}$  and  $\bar{()^s}$  are conservative:

$$\sum_{\ell=0}^N \bar{f}_{\ell+1/2}^r \Delta z_{\ell+1/2} = \sum_{\ell=1}^N f_{\ell} \Delta z_{\ell}, \tag{B13}$$

$$\sum_{\ell=1}^N \bar{g}_{\ell}^s \Delta z_{\ell} = \sum_{\ell=0}^N g_{\ell+1/2} \Delta z_{\ell+1/2}, \tag{B14}$$

$$\sum_{\ell=0}^N \bar{f}_{\ell+1/2}^r g_{\ell+1/2} \Delta z_{\ell+1/2} = \sum_{\ell=1}^N f_{\ell} \bar{g}_{\ell}^s \Delta z_{\ell}. \tag{B15}$$

(ii) Average of a derivative:

$$\left. \frac{\partial \bar{g}^p}{\partial z} \right|_{\ell+1/2} = \bar{\left. \frac{\partial g}{\partial z} \right|_{\ell+1/2}}^r, \tag{B16}$$

$$\left. \frac{\partial \bar{f}^w}{\partial z} \right|_{\ell} = \bar{\left. \frac{\partial f}{\partial z} \right|_{\ell}}^s. \tag{B17}$$

(iii) Derivative of a product:

$$\begin{aligned} \left. \frac{\partial (gh)}{\partial z} \right|_{\ell} &= \bar{h}_{\ell}^p \left. \frac{\partial g}{\partial z} \right|_{\ell} + \bar{g}_{\ell}^s \left. \frac{\partial h}{\partial z} \right|_{\ell} \\ &= \bar{h}_{\ell}^s \left. \frac{\partial g}{\partial z} \right|_{\ell} + \bar{g}_{\ell}^p \left. \frac{\partial h}{\partial z} \right|_{\ell}, \end{aligned} \tag{B18}$$

$$\begin{aligned} \left. \frac{\partial (ef)}{\partial z} \right|_{\ell+1/2} &= \bar{e}_{\ell+1/2}^w \left. \frac{\partial f}{\partial z} \right|_{\ell+1/2} + \bar{f}_{\ell+1/2}^r \left. \frac{\partial e}{\partial z} \right|_{\ell+1/2} \\ &= \bar{e}_{\ell+1/2}^r \left. \frac{\partial f}{\partial z} \right|_{\ell+1/2} + \bar{f}_{\ell+1/2}^w \left. \frac{\partial e}{\partial z} \right|_{\ell+1/2}, \end{aligned} \tag{B19}$$

$$\left. \frac{\partial (\bar{f}^w \bar{g})}{\partial z} \right|_{\ell} = f_{\ell} \left. \frac{\partial g}{\partial z} \right|_{\ell} + \bar{g}_{\ell}^s \left. \frac{\partial f}{\partial z} \right|_{\ell}, \tag{B20}$$

$$\left. \frac{\partial(\bar{g}^p f)}{\partial z} \right|_{\ell+1/2} = g_{\ell+1/2} \left. \frac{\partial f}{\partial z} \right|_{\ell+1/2} + f \left. \frac{\partial \bar{g}^r}{\partial z} \right|_{\ell+1/2}. \quad (\text{B21})$$

A particularly useful result is that if  $p$ -level masses  $m_\ell$  (here  $\ell$  is a level index) satisfy a discrete conservation equation with vertical fluxes  $F_{\ell+1/2}$

$$\frac{\partial m_\ell}{\partial t} + \frac{\partial F}{\partial z} \Big|_\ell = \dots, \quad (\text{B22})$$

then Equation (B16) implies that the  $\bar{m}_{\ell+1/2}^r$  satisfy a discrete conservation equation with vertical fluxes  $\bar{F}_\ell^p$

$$\frac{\partial \bar{m}_{\ell+1/2}^r}{\partial t} + \frac{\partial \bar{F}^p}{\partial z} \Big|_{\ell+1/2} = \dots. \quad (\text{B23})$$

This vertically averaged discrete mass conservation equation can then be used as the basis for discrete  $w$ -level tracer conservation equations for  $(\bar{m}^r \eta)_\ell$  and  $(\bar{m}^r q)_\ell$ ; for example:

$$\frac{\partial}{\partial t} (\bar{m}_{\ell+1/2}^r q_{\ell+1/2}) + \frac{\partial}{\partial z} (\bar{F}^p q^{\text{adv}}) \Big|_{\ell+1/2} = \dots, \quad (\text{B24})$$

where  $q^{\text{adv}}$  is the value of  $q$  used in computing the advective flux. The tracer conservation equations are consistent in the sense that they reduce to the  $w$ -level mass conservation equation when the tracer value is constant and right-hand side terms vanish.